UNIVERSIDADE DA BEIRA INTERIOR
Engenharia

Robust nonlinear feedback control for Rendezvous in near-circular orbits

(Versão corrigida após defesa)

Eduardo David Godinho

Dissertação para obtenção do Grau de Mestre em
Engenharia Aeronáutica

(ciclo de estudos integrado)

Orientador: Prof. Doutor Kouamana Bousson

Covilhã, janeiro de 2020

Acknowledges

This dissertation could not have been done without the help and support of my family and friends to whom I heartfully thank. It is also with great pleasure that I thank Professor Kouamana Bousson for guiding me on this journey and for taking his time to help me and to share his knowledge.

Resumo

O crescente desenvolvimento do setor espacial tem vindo a impulsionar novas tecnologias e métodos inovadores. Um destes métodos, o rendezvous orbital, está presente desde a década de 60, e consiste em aproximar dois veículos espaciais, um deles passivo denominado de "target" e o outro ativo denominado de "chaser". Este segundo, por sua vez, executa manobras com o auxílio de propulsores de modo a reduzir a distância relativa entre os dois veículos até que esta seja aproximadamente nula. Inicialmente, este processo era feito manualmente, no entanto, atualmente, a tecnologia progrediu de tal forma que o processo consegue ser completamente autónomo. No início da automação desta manobra espacial, a preocupação seria apenas completar a missão, contudo esta progrediu no sentido de melhorar este processo de automação tendo em conta o consumo de propelente e a quantidade de tempo gasto. Desta forma, a presente dissertação tem como objetivo desenvolver e implementar um controlador robusto, baseado numa metodologia de Lyapunov, de modo a mostrar a sua performance, robustez e eficácia numa missão de rendezvous orbital. Ao utilizar um sistema linear dinâmico em que a excentricidade da órbita do "target" se assume como uma incerteza do sistema, o controlador não-linear consegue criar uma trajetória suave, para que o "chaser" se aproxime do "target". Os resultados obtidos demonstram que este controlador consegue encontrar a solução para o problema de rendezvous tanto para pequenas distâncias e velocidades relativas assim como para grandes, gerando sempre trajetórias suaves sem ultrapassar o "target". Verifica-se também que, mesmo perturbando o sistema com a incerteza, o controlador consegue gerar uma trajetória robusta com ótimos resultados. Este tipo de controlador para missões de rendezvous, para além de ser robusto e eficaz, como demonstrado nos resultados obtidos, consegue gerar ótimos resultados para rendezvous entre órbitas não-coplanares não-circulares.

Palavras-chave

Lyapunov; Rendezvous espacial; Robustez; Não-coplanares.

Abstract

The growing development of the space sector has been driving new technologies and innovative methods. One of these methods, the orbital rendezvous, has been around since the 1960s and consists of bringing together two spacecrafts, one of them is passive, named "target", and the other is active, called the "chaser". This second spacecraft, in turn, performs maneuvers with the aid of thrusters in order to reduce the relative distance between the two vehicles until it is approximately zero. Initially, this process was done manually, however, today technology has progressed such that the process can be completely autonomous. At the beginning of the automation of this space maneuver, the concern would only be to complete the mission, however, it has progressed towards improving this automation process taking into account propellant consumption and the amount of time spent to perform it. Thus, the present dissertation aims to develop and implement a robust controller, based on a Lyapunov's approach, to show its performance, robustness, and effectiveness in an orbital rendezvous mission. By using a linear dynamic system, where the orbital eccentricity of the target is assumed to be a system uncertainty, the nonlinear controller can create a smooth trajectory so that the chaser approaches the target. The results show that this nonlinear controller can find the solution to the problem of rendezvous for short relative distances and low relative speeds as well as for large, always generating smooth paths without overshooting the target. It was also found that even by disturbing the system with uncertainty, the controller can generate a robust trajectory with great results. This type of controller for rendezvous missions, besides being robust and effective, as demonstrated in the obtained results, can generate excellent results for rendezvous between non-circular non-coplanar orbits.

Keywords

Lyapunov; Orbital Rendezvous; Robustness; Non-coplanar.

Contents

List of Figures

List of Tables

List of Acronyms

ATV	Automated Transfer Vehicle
CARE	Continuous Algebraic Riccati Equation
GPS	Global Positioning System
HTV	H-II Transfer Vehicle
ISS	International Space Station
LOS	Line of Sight
ODE	Ordinary Differential Equations
PVT	Position, Velocity and Time
RND	Rendezvous and Docking
SGRA	Sequential Gradient Restoration Algorithm
USSR	Union of Soviet Socialist Republics

Nomenclature

Symbols	Description	System of Units
Δ	Uncertainty set	$[-]$
ΔA	Uncertain perturbation of the nominal system A	$[-]$
μ	Gravitational parameter	$[m^3 \cdot s^{-2}]$
π	Pi	$[-]$
ϕ	Control law	$[-]$
ω	Mean motion of the target	$[rad \cdot s^{-1}]$
A	State matrix	$[-]$
B	Control matrix	$[-]$
C	Output matrix	$[-]$
D	Feedthrough matrix	$[-]$
E	Eccentric anomaly of the target spacecraft	$[rad]$
H	Hamiltonian	$[-]$
I	Identity matrix	$[-]$
J	Performance functional	$[-]$
M	Mean anomaly of the target spacecraft	$[rad]$
M_2	Algebraic modified equation solution	$[-]$
P	Algebraic modified equation solution	$[-]$
R_1	State weighting matrix	$[-]$
R_2	Control weighting matrix	$[-]$
$\hat{R}_2$	Additional state weighting matrix	$[-]$
T	Time-step	$[s]$
T	Orbital period	$[s]$
V	Lyapunov's function	$[-]$
$\mathcal{C}$	Controllability matrix	$[-]$
$\mathcal{O}$	Observability matrix	$[-]$
$\mathbb{N}$	Set of nonnegative-definite matrices	$[-]$
$\mathbb{P}$	Set of positive-definite matrices	$[-]$
$\mathbb{R}$	Set of real numbers	$[-]$
a	Thrust acceleration	$[m \cdot s^{-2}]$
a	Semimajor axis	$[m]$
e	Eccentricity	$[-]$
f	Control force	$[N]$
h	Specific relative angular momentum	$[m^2 \cdot s^1]$

m	Mass of the chaser spacecraft	$[kg]$
n	Mean motion of the target	$[rad \cdot s^{-1}]$
o	Center of mass of the target spacecraft	$[m]$
r	Position along a Keplerian orbit	$[m]$
$\ddot{r}$	Vector acceleration	$[m \cdot s^{-2}]$
r_a	Apogee distance	$[m]$
r_p	Perigee distance	$[m]$
t	Time	$[s]$
$u(t)$	Control input vector	$[-]$
x	Relative position along the x-axis	$[m]$
$\dot{x}$	Relative velocity along the x-axis	$[m \cdot s^{-1}]$
$\ddot{x}$	Relative acceleration along the x-axis	$[m \cdot s^{-2}]$
$x(t)$	State vector	$[-]$
$\dot{x}(t)$	State differential equation	$[-]$
y	Relative position along the y-axis	$[m]$
$\dot{y}$	Relative velocity along the y-axis	$[m \cdot s^{-1}]$
$\ddot{y}$	Relative acceleration along the y-axis	$[m \cdot s^{-2}]$
$y(t)$	Output vector	$[-]$
z	Relative position along the z-axis	$[m]$
$\dot{z}$	Relative velocity along the z-axis	$[m \cdot s^{-1}]$
$\ddot{z}$	Relative acceleration along the z-axis	$[m \cdot s^{-2}]$

Superscripts	**Description**
T	Transpose matrix

Subscripts	**Description**
0	Initial
f	Final
max	Maximum
p	Perigee
x	Component along the x-axis
y	Component along the y-axis
z	Component along the z-axis

Chapter 1 - Introduction

Since the dawn of mankid, the sky and the space beyond have always been a cause of wonder. Initially adopted by men to guide them on the discovery of new worlds on Earth, space turned out to be a profitable way of making business and testing new technologies. It all started out with Sputnik-1, a very simple USSR satellite, with the objective of demonstrating launching and orbiting capabilities of the Sputnik program. From there it started the famous space race that boosted space exploration which led to massive investments on space technology. No more than 8 years later, the first successful rendezvous mission took place with the spacecrafts Gemini 6 and Gemini 7. Later on, the moon landing happened, becoming a milestone in space exploration. Subsequently, new space programs such as the International Space Station (ISS), the Space Shuttle and the Mir Station were launched.

Currently, the continued presence in space has been established, starting with the assembly of the ISS. Maintaining and delivering supplies and/or astronauts to this facility is an ongoing process that requires performing a successful rendezvous and docking maneuver. The orbital rendezvous and docking process was initially performed manually, i.e., by the spacecraft's crew or by a ground station. By doing so, many safety issues would arise, and the mission's success could be compromised. In order to overcome this problem and to guarantee the human factor is not a risk to the mission, some spacecrafts such as the European automated transfer vehicle (ATV) and the Japanese H-II Transfer Vehicle (HTV) both unmanned, rely on an absolute GPS navigation based on position, velocity and time (PTV) filtering that provides the absolute position estimation with the accuracy required by the specific relative GPS processing.

More recently, the SpaceX Dragon was appointed to deliver cargo, making it the first-ever reusable cargo spacecraft. Following this development, Dragon-2 is currently being tested to perform fully automated RND's delivering cargo and/or personnel to the ISS.

In the future, RND operations may be used to refuel spacecrafts, on-orbit, for interplanetary expeditions, making access to space more affordable.

Figure 1.1: SpaceX Dragon-2 docking with the ISS.

1.1 Orbital Rendezvous and Docking Operations

The orbital rendezvous is one of the many maneuvers performed by spacecrafts during their missions. The rendezvous maneuver implies a pre-determined meeting between two spacecrafts, the chaser and the target spacecrafts, with a specific mission (delivering supplies and/or personal, maintenance, etc.), where the two entities' relative position and velocity approximate to zero. The designations "chaser" and "target" are assigned based on the use of thrusters to perform the orbital maneuver, where the chaser is classified as "active" and the target is classified as "passive" regarding the use of its propulsion system to complete the task at hand. In some cases, the target can also use thrusters in the orbital rendezvous, in which case its classification changes to "active".

Regarding human space activities, the rendezvous maneuver is, most of the time, hand to hand with the docking maneuver, where the first one is needed for the second one to be accomplished. A typical rendezvous and docking maneuver (RND) can be divided into five stages named launch, phasing, close-range rendezvous, final approaching, and docking. The close-range rendezvous is then subdivided into the homing and closing phases.

The launch stage starts when the chaser is launched into space with the intent to perform an orbital rendezvous. The following phase, the phasing stage, where the main goal is to start the relative navigation using the ground telemetry tracking and command network, requiring the chaser to detect the target, is achieved by carrying out several maneuvers to reduce the orbital plane differences, to adjust the phase angle between the chaser and the target and to increase the orbital height.

In the homing phase, the aim is to autonomously attain the target's orbit and to reduce the chaser's relative velocity, where the phase's final position is only a couple of kilometers away from the target and denominated a station-keeping point, a location where orbital maneuvers are executed in order to keep a spacecraft in an assigned orbit.

In the closing phase, the chaser gets to another station-keeping point located a few hundred meters away from the target. Finally, to complete the RND maneuver, the final approaching phase takes place, where the chaser approaches the target along a straight line, satisfying the

relative position, velocity, attitude and angular rate requirements for the docking. The procedure is completed when the chaser touches the target. Figure 1.2 illustrates a typical RND process, as described above.

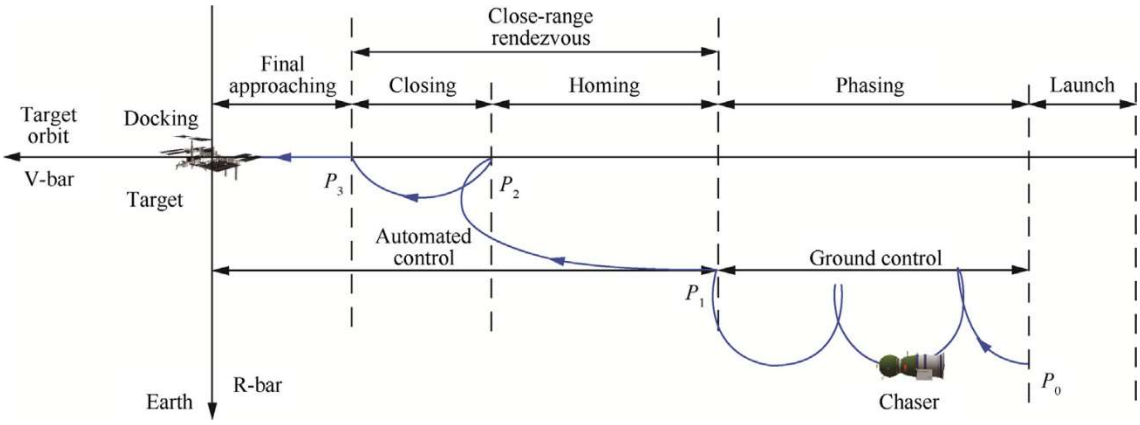

Figure 1.2: Spacecraft rendezvous and docking process.

1.2 Rendezvous Guidance Schemes

RND maneuvers have always been a hard challenge to overcome throughout space missions' history. In the early years, for the Apollo Lunar Landing program, the focus of the rendezvous guidance systems was mostly on coplanar and near-circular orbits, while in close proximity, making them only relevant for the terminal rendezvous phase. Those systems would rely on the positions and velocities of the two spacecrafts in a common frame and would employ continuous corrections while canceling the angular rate of the line of sight (LOS) by applying a thrust normal to the vector connecting the two spacecrafts. Some early studies mainly focused on the optimization of linear rendezvous trajectories, i.e., the propellant-optimal linear impulse rendezvous problem. Lawden [1] proposed the use of primer-vector theory of impulse maneuvers, based on the Pontryagin maximal principle, while also providing the first-order conditions for propellant-optimal trajectories. Lion and Handelsman [2] later improved the primer-vector theory to the non-optimal primer-vector theory by adding maneuver or coasting arcs, showing that a trajectory not satisfying Lawden's first-order conditions could be improved to an optimal one. More recently, Wang et al. [3] extended the primer-vector theory to help optimize a four-impulse elliptical rendezvous trajectory while many studies tried to deal with propellant-optimal, time and trajectory optimizations became a concern too. Miele et al. [4] used a sequential gradient-restoration algorithm (SGRA) to obtain time-optimal and fuel-optimal solutions for the rendezvous problem in a circular orbit.

Until recently, almost all the solutions to deal with the rendezvous problem assume the target's orbit to be perfectly circular, which isn't the case in the real world. To deal with this gap, Wan et al. [5] developed a robust guaranteed cost observer-controller in near-circular orbits using the noncircularity of the target orbit as a parametric uncertainty. Furthermore, a multi-objective robust H_∞ controller [6] was also proposed to solve the rendezvous problem of

two neighboring spacecrafts exposed to parameter uncertainties and external perturbations, using a Lyapunov approach. Although H_∞ guarantees robustness, since it takes into consideration that the worst possible disturbance cannot destabilize the system, performance objectives may not be fulfilled such as time-optimal and/or fuel-optimal solutions. To guarantee robust stability and performance, Haddad et al. [7] suggest a generalization of the classical Hamilton-Jacobi-Bellman conditions to deal with the design of robust nonlinear optimal controllers for uncertain linear systems. Such a controller is attained by modifying the nonlinear-nonquadratic performance criterion to account for system uncertainty.

Going even further, studies on the rendezvous problem started to account for perturbations such as the aerodynamic drag and Earth oblateness. Park et al. [8] used a two-step sliding mode control in the presence of the earth's gravitational perturbation while minimizing the amount of delta-v needed to perform the rendezvous. Further, Pernicka et al. [9] proposed optimal techniques for determining translational and rotational maneuvers that simplify the RND process, while considering the Earth oblateness, more precisely, the J_2 perturbation.

The tides shifted from having guidance controls where the goal was to have a successful mission, independently of the propellant consumption, to having precise systems that account for time, fuel and trajectory optimizations while under perturbations, and they will, most likely, progress to even more precise and safer systems.

1.3 Objectives and Contributions

The present dissertation aims to demonstrate the robustness and performance of a nonlinear control when applied to a dynamic linear model of a rendezvous problem where the chaser spacecraft performs a rendezvous maneuver in a near-circular orbit. A first-order relative uncertain motion model in near-circular orbit is employed to account for the noncircularity of the target orbit as a parametric uncertainty. Following the controller design, four simulations will be made to generate four numerical examples to be examined and compared. The first three examples will demonstrate the controller robustness for a range of relative distances and velocities while the last one will demonstrate that the controller can still deliver great results even when perturbations are added to the system.

The present framework intents to find safer and more reliable solutions for the growing need for new controllers on RND operations.

1.4 Layout of the Dissertation

The present dissertation is divided into five chapters, where each one provides detailed information regarding current methodologies, used algorithm, results and so one.

The first chapter is used as an introduction to the dissertation, briefly explaining the concept of Rendezvous and Docking, mentioning current methodologies applied to rendezvous problem and commenting on the objectives and contributions of the present dissertation.

The second chapter describes the relative motion model and the coordinate system that was used, while presenting the progress on the relative dynamic equations, from the basic to the point where it takes into account parametric uncertainty.

The third chapter explains how to obtain the nonlinear control law for the rendezvous problem using a Lyapunov based approach, briefly describing the concepts of linear systems, and feedback control while also explaining the used methodology in the current dissertation.

The fourth chapter presents the results obtained using the designed controller in the previous chapter, presenting four examples, three with no perturbations and one with, where comments are made regarding robustness, performance, and efficiency of the nonlinear controller.

The fifth and last chapter presents a brief summary of the dissertation, stating its objectives, used methodology, obtained results and future perspectives.

Chapter 2 – Dynamic Model

Man has always tried to translate natural phenomena into a language that he comprehends best. From fields such as biology to mathematics and physics, models have been made to understand and portray what surrounds the human species. The space beyond Earth's atmosphere is no exception, therefore, many models were created to represent, as accurate as possible, the mechanisms that rule in such a harsh environment.

2.1 Coordinate System

To formulate the rendezvous problem and to define its dynamical model a coordinate system must be chosen first. A local vertical local horizontal (LVLH) frame centered on the target spacecraft is used, where the x-axis, also called R-bar, is directed radially outward along the position vector r, centered on Earth, the y-axis, also called V-bar, is along the velocity direction and the z-axis, also called H-bar is normal to the reference orbit plane. Figure 2.1 illustrates the coordinate system described above.

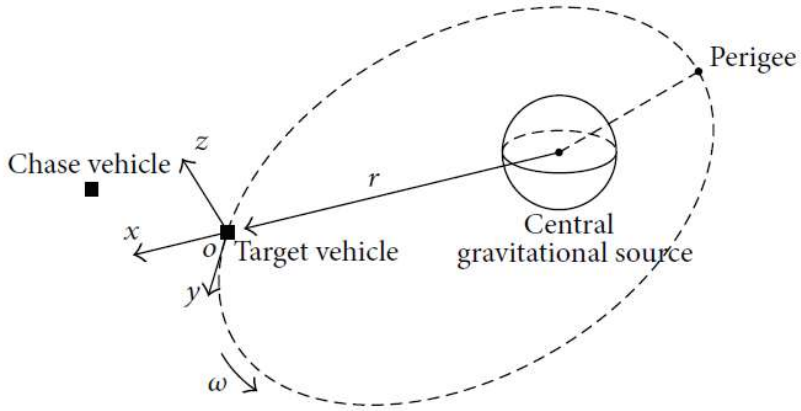

Figure 2.1: Local vertical local horizontal frame.

2.2 Relative Motion Model

2.2.1 Basic relative dynamics equations

On the early steps of the RND breakthrough, only basic orbital relative motion models existed. Clohessy and Wiltshire [10] developed one of them in which state that when two spacecrafts, orbiting the same body in near-circular orbits, have a relative distance much shorter than the spacecraft's geocentric distance, while ignoring orbital perturbations, the relative motion can be described by the following set of linear dynamics equations

$$\begin{cases} \ddot{x} + 2\dot{\omega}y + 3\omega^2 x = a_x \\ \ddot{y} - 2\omega\dot{x} = a_y \\ \ddot{z} + \omega^2 z = a_z \end{cases} \quad (2.1)$$

where ω is the orbital angular rate of the target and a_x, a_y and a_z are the thrust acceleration components on each axis. The Clohessy-Wiltshire equations also referred to as the Hill equations, have a closed-form analytical solution that allows the relative motion to be divided into two different parts, the in-plane motion (x-y plane) and the out-of-plane motion (z-direction). Also, by looking at the equation set, it is noticeable that only the motion in the directions of x and y are coupled with each other. Furthermore, when the control forces are removed, the out-of-plane trajectory waves as a trigonometric function and the in-plane trajectory relates closely to its initial state.

2.2.2 Relative dynamics equations with parametric uncertainty

When the chaser spacecraft experiences an additional perturbing force f, the set of equations that describes the relative motion using a cartesian referential can be derived as [11]

$$\begin{cases} \ddot{x} = \frac{2\mu}{r^3}x + \dot{\omega}y + \omega^2 x + 2\omega\dot{y} + \frac{f_x}{m} \\ \ddot{y} = -\frac{\mu}{r^3}y - \dot{\omega}x + \omega^2 y - 2\omega\dot{x} + \frac{f_y}{m} \\ \ddot{z} = -\frac{\mu}{r^3}z + \frac{f_z}{m} \end{cases} \quad (2.2)$$

where μ is the gravitational parameter, f_x, f_y and f_z are the components of the control force f and m is the mass of the chaser spacecraft. Wan et al. [11] also used a generalized Langrage's expansion theorem to further linearize the equation set (2.2) to allow for the use of linear control theory. Furthermore, the equation set (2.2) was rewritten as the functions of the eccentric anomaly of the target spacecraft, E, the mean anomaly of the target spacecraft, M, the time of periapsis passage, t_p, and the eccentricity of the target orbit, e, according to the conversions between the orbital parameters and Kepler's time equation

$$E = M + e\sin(E) \quad (2.3)$$

$$M = n(t - t_p) \quad (2.4)$$

where t is an arbitrary time and n is the mean motion defined as

$$n = \sqrt{\frac{\mu}{a^3}} \quad (2.5)$$

with a being the semimajor axis of the target orbit. Wan also states that when the eccentricity of the target orbit is sufficiently small, the nonlinear terms can be expanded as power series in constant e. By truncating at order e, the following linearized results are obtained in a Keplerian referential

$$\frac{\mu}{r^3} = n^2\left(\frac{a}{r}\right)^3 = n^2\left(\frac{1}{1-e\cos E}\right)^3 \approx n^2(1+3e\cos M) \quad (2.6)$$

$$\omega = \frac{h}{r^2} = n\left(\frac{1}{1-e\cos E}\right)^2 \approx n(1+2e\cos M) \quad (2.7)$$

$$\omega^2 = \left(\frac{h}{r^2}\right)^2 = n^2\left(\frac{1}{1-e\cos E}\right)^4 \approx n^2(1+4e\cos M) \quad (2.8)$$

$$\dot{\omega} = \frac{-2h}{r^3} = -2n^2\frac{e\sin E}{(1-e\cos E)^4} \approx -2en^2\sin M \quad (2.9)$$

where h and r are the angular momentum and the radius of the target orbit, respectively. Next, the state vector can be defined as

$$x(t) = [x, y, z, \dot{x}, \dot{y}, \dot{z}]^T \quad (2.10)$$

and the control vector as

$$u(t) = \left[f_x, f_y, f_z,\right]^T \quad (2.11)$$

Now, by substituting (2.6)-(2.9) into the equation set (2.2), the first-order relative motion model for rendezvous in near-circular orbits can be rewritten in a matrix form as

$$\dot{x}(t) = (A + \Delta A)x(t) + Bu(t) \quad (2.12)$$

where matrices $A, \Delta A$, and B are defined as

$$A = \begin{bmatrix} 0 & 0 & 0 & 1 & 0 & 0 \\ 0 & 0 & 0 & 0 & 1 & 0 \\ 0 & 0 & 0 & 0 & 0 & 1 \\ 3n^2 & 0 & 0 & 0 & 2n & 0 \\ 0 & 0 & 0 & -2n & 0 & 0 \\ 0 & 0 & -n^2 & 0 & 0 & 0 \end{bmatrix} \quad B = \frac{1}{m}\begin{bmatrix} 0 & 0 & 0 \\ 0 & 0 & 0 \\ 0 & 0 & 0 \\ 1 & 0 & 0 \\ 0 & 1 & 0 \\ 0 & 0 & 1 \end{bmatrix}$$

$$\Delta A = \begin{bmatrix} 0 & 0 & 0 & 0 & 0 & 0 \\ 0 & 0 & 0 & 0 & 0 & 0 \\ 0 & 0 & 0 & 0 & 0 & 0 \\ 10en^2\cos M & -2en^2\sin M & 0 & 0 & 4en\cos M & 0 \\ 2en^2\sin M & en^2\cos M & 0 & -4en\,cos\,M & 0 & 0 \\ 0 & 0 & -3en^2\cos M & 0 & 0 & 0 \end{bmatrix} \quad (2.13)$$

The norm-bounded matrix ΔA defined as $\exists\ \lambda > 0$: $\|\Delta A\|^2{}_F \leq \lambda$ that contains eccentricity of the target orbit is defined as the noncircular model uncertainty. By using this motion model, the controller to be designed will be simpler and more robust. Furthermore, since most rendezvous missions are conducted in near-circular orbits, the present model is more accurate for engineering applications. Also, comparing it with the equation set (2.2), the near-circular-orbit model is more precise, which can guarantee robustness and better performance on the controller implementation. Additionally, this kind of relative motion model makes the controller design easier than a controller based on elliptical-orbit models.

Chapter 3 – Nonlinear Control Law for The Rendezvous Problem

Guidance and control of RND operations has always been a case of study since the early days of spaceflight. As mentioned before, the rendezvous problem progressed from the mission's successfulness to its optimization, by either minimizing fuel or time or a combination of the two.

Currently, many techniques have been applied to solve the rendezvous control problem. Most use real-time computations, on-line or off-line, to generate a priori trajectories plans to be further implemented during RND operations. The present chapter presents a brief introductory explanation of linear dynamic systems, Lyapunov's theory and feedback control for a better understanding of the rendezvous controller formulation.

3.1 Linear Dynamic System

A system is merely a collection of elements that interact with its environment using a set of input variables u and output variables y. Going further, systems can be classified as static or dynamic. A system is said to be static if its output depends only on its present input, i.e. there exists a function $f(u,t)$ such that for all $t \in T$,

$$y(t) = f(u(t),t) \quad (3.1)$$

In contrast, a dynamic system requires past input to determine the system output, i.e., there exists a function $f(x,u,t)$ and a function $h(x,u,t)$ such that

$$\dot{x} = f(x(t),u(t),t) \quad (3.2)$$
$$y = h(x(t),u(t),t) \quad (3.3)$$

where x and u represent the state and control variables, respectively. Most common systems take the form

$$\dot{x} = A(t)x + B(t)u \quad (3.4)$$
$$y = C(t)x + D(t)u \quad (3.5)$$

where $x(t) \in \mathbb{R}^n, u: [0,\infty) \to \mathbb{R}^m$ and $y: [0,\infty) \to \mathbb{R}^p$. $A(t)$ is the $n \times n$ state matrix, $B(t)$ is the $n \times m$ input matrix, $C(t)$ is the $p \times n$ output matrix and $D(t)$ is the $p \times m$ feedthrough matrix

and can be obtained from the Jacobian linearization of a nonlinear system such as the one described in (3.2) and (3.3).

3.2 Feedback control

To control a system is to make its variables obey to a particular value, commonly called the reference value. This control can assume two types, the open-loop control, in which the system does not measure the output and there is no correction of the actuating signal to make sure it leads the system to the reference value and the closed-loop (feedback) control, in which the system includes a sensor to measure the output and uses the feedback of the sensed value to impact the control variable.

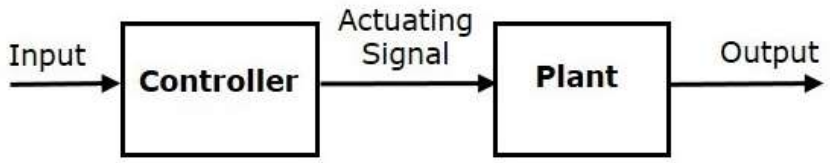

Figure 3.1: Diagram of an open-loop system.

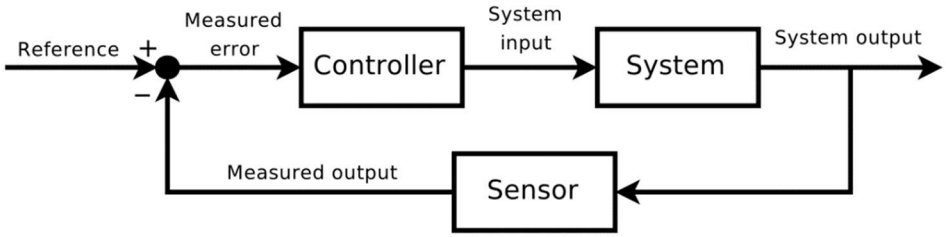

Figure 3.2: Diagram of a closed-loop system.

3.3 Controllability and Observability

Having a linear dynamic system, it is not enough to state that it can even be controlled or if it can even be observed. Kalman introduced these two concepts stating that controllability is concerned with whether one can design control input to steer the state to arbitrary values and observability is concerned with whether without knowing the initial state, one can determine the state of a system given the input and the output.

3.3.1 Controllability

Considering a system in the state-space form described by equations (3.4) and (3.5), the system is controllable if and only if the controllability matrix

$$\mathcal{C} = [B \quad AB \quad A^2B \quad \dots \quad A^{n-1}B] \qquad (3.6)$$

has $rank(\mathcal{C}) = n$.

3.3.2 Observability

Just like controllability, the observability of a system can be checked using a similar test. Given the same system in the state-space form described by equations (3.4) and (3.5), the system is observable if and only if the observability matrix

$$\mathcal{O} = \begin{bmatrix} C \\ CA \\ CA^2 \\ \vdots \\ CA^{n-1} \end{bmatrix} \quad (3.7)$$

has $rank(\mathcal{O}) = n$.

3.4 Lyapunov Stability Theory

With the observability and controllability concepts, one has tools to survey the linear dynamic system, but it still fails to have the tools to control it. One way to control a system is by using a point of equilibrium where the stability of solutions near it is assessed. Lyapunov stability theory uses this principle by providing a means of stabilizing unstable nonlinear systems using feedback control. By selecting a suitable Lyapunov function and force it to decrease along the trajectory of the system, one can converge the system to its equilibrium. This rate of convergence to the equilibrium can also be controlled by forcing the Lyapunov function to decrease to zero faster. To illustrate this theory, consider the general nonlinear autonomous dynamical system

$$\dot{x}(t) = f\big(x(t)\big), \qquad x(0) = x_0 \quad (3.8)$$

From this system, six different types of stability can be observed:

- The zero solution $x(t) \equiv 0$ to (3.8) is Lyapunov stable if, for all $\varepsilon > 0$, there exists $\delta = \delta(\varepsilon) > 0$ such that if $\|x(0)\| < \delta$, then $\|x(t)\| < \varepsilon, t \geq 0$;

- The zero solution $x(t) \equiv 0$ to (3.8) is locally asymptotically stable if it is Lyapunov stable and there exists $\delta > 0$ such that if $\|x(0)\| < \delta$, then $\lim_{t\to\infty} x(t) = 0$;

- The zero solution $x(t) \equiv 0$ to (3.8) is locally exponentially stable if there exist positive constants α, β and δ such that if $\|x(0)\| < \delta$, then $\|x(t)\| \leq \alpha\|x(0)\|e^{-\beta t}, t \geq 0$;

- The zero solution $x(t) \equiv 0$ to (3.8) is globally asymptotically stable if it is Lyapunov stable and for all $x(0) \in \mathbb{R}^n$, $\lim_{t\to\infty} x(t) = 0$;

- The zero solution $x(t) \equiv 0$ to (3.8) is globally exponentially stable if there exist positive constants α, β and δ such that if $\|x(0)\| < \delta$, then $\|x(t)\| \leq \alpha \|x(0)\| e^{-\beta t}, t \geq 0$, for all $x(0) \in \mathbb{R}^n$;

- Finally, the zero solution $x(t) \equiv 0$ to (3.8) is unstable if it is not Lyapunov stable.

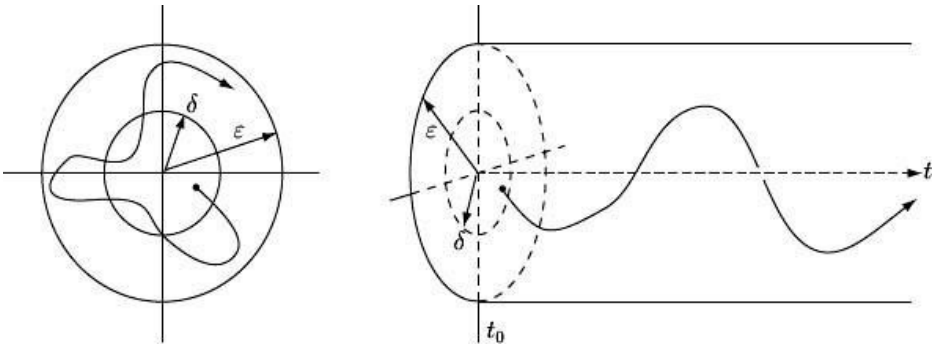

Figure 3.3: Lyapunov stability of an equilibrium point.

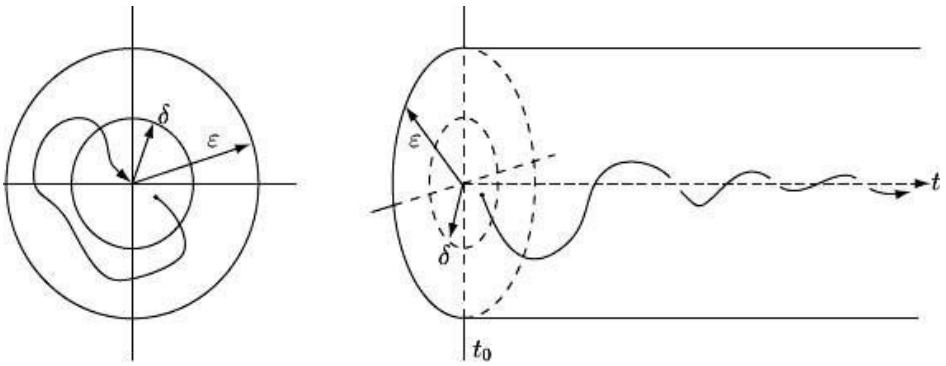

Figure 3.4: Asymptotic stability of an equilibrium point.

Figure 3.5 portrays the comparison between three different types of stability

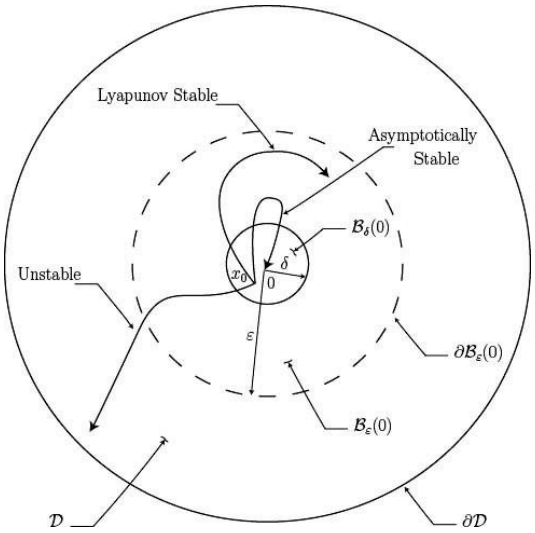

Figure 3.5: Asymptotically stable, Lyapunov stable and unstable equilibrium points.

As for the Lyapunov function, it is a scalar function $V: \mathcal{D} \to \mathbb{R}$ such that

$$V(0) = 0 \quad (3.9)$$

$$V(x) > 0,\ x \in \mathcal{D},\ x \neq 0 \quad (3.10)$$

$$V'(x)f(x) \leq 0, \quad x \in \mathcal{D} \quad (3.11)$$

and has a continuous first-order partial derivates at every point of $\mathcal{D}$. The existence of this function guarantees the Lyapunov stability of the zero solution $x(t) \equiv 0$. In addition, if

$$V'(x)f(x) < 0,\ x \in \mathcal{D},\ x \neq 0 \ (3.12)$$

then the zero solution $x(t) \equiv 0$ to (3.8) is asymptotically stable. Furthermore, if there exist scalars $\alpha, \beta, \varepsilon > 0$ and $p \geq 1$ such that $V: \mathcal{D} \to \mathbb{R}$ satisfies

$$\alpha\|x\|^p \leq V(x) \leq \beta\|x\|^p,\ x \in \mathcal{D} \ (3.13)$$

$$V'(x)f(x) \leq -\varepsilon V(x),\ x \in \mathcal{D} \ (3.14)$$

then the zero solution $x(t) \equiv 0$ to (3.8) is exponentially stable. Next, considering the Lyapunov function candidate $V(x) = x^T P x$ where $x \in \mathbb{R}^n$ and $P \in \mathbb{R}^{n \times n}$ is positive definite, note that

$$\dot{V}(x) = V'(x)f(x) = 2x^T PAx = x^T(A^T P + PA)x \ (3.15)$$

and if there exists a nonnegative-definite matrix $R \in \mathbb{R}^{n \times n}$ such that $A^T P + PA = -R$ so that $V'(x)f(x) = -x^T Rx \leq 0$, then it is useful to determine the existence of a positive-definite matrix P satisfying, what is called, a Lyapunov equation

$$0 = A^T P + PA + R \ (3.16)$$

Also, if $R = C^T C$ where $C \in \mathbb{R}^{l \times n}$, and assuming (A, C) is observable, then the zero solution $x(t) \equiv 0$ to (3.8) is globally asymptotically stable if and only if there exists a unique positive-definite matrix $P \in \mathbb{R}^{n \times n}$ satisfying

$$0 = A^T P + PA + C^T C \ (3.17)$$

3.5 Problem Formulation

From the concepts and conditions mentioned above, the orbital rendezvous problem can now be properly framed. In this section, to generate a nonlinear feedback control for a linear system a transparent generalization of the Hamilton-Jacobi-Bellman conditions for time-invariant and infinite horizon problems is used.

Firstly, let $D \subset \mathbb{R}^n$ be an open set and let $C \subset \mathbb{R}^m$ where $0 \subset D$ and $0 \subset C$. Furthermore, let $\tilde{\mathcal{F}} \subset \{\tilde{f}: D \times C \to \mathbb{R}^n: \tilde{f}(0,0) = 0\}$ represent the class of uncertain closed-loop nonlinear systems where $\tilde{f}_0(\cdot,\cdot) \in \tilde{\mathcal{F}}$ defines the nominal nonlinear system. To tackle the rendezvous problem, the following uncertain system must be controlled

$$\dot{x} = \tilde{f}\big(x(t), u(t)\big), \;\; x(0) = x_0, \qquad t \geq 0 \qquad (3.18)$$

where the control $u(\cdot)$ is limited to the class of admissible controls such that $u(t) \in U$, for all $t \geq 0$, with a control law $\phi(\cdot)$ that takes the form of a feedback control $u(t) = \phi\big(x(t)\big)$ and minimizes the performance functional

$$\tilde{J}_{\tilde{f}}\big(x_0, u(\cdot)\big) \triangleq \int_0^\infty \tilde{L}\left(x(t), u(t)\right) dt \qquad (3.19)$$

The closed-loop system is now defined as

$$\dot{x} = \tilde{f}\left(x(t), \phi\big(x(t)\big)\right), \;\; x(0) = x_0, \qquad t \geq 0 \qquad (3.20)$$

and it is assumed that it has a unique solution forward in time.

3.6 Theoretical Method

The next step is to describe robust feedback controllers that guarantee robust stability over a class of nonlinear uncertain systems and minimize an auxiliary performance functional, thus using the Hamilton-Jacobi-Bellman conditions.

Firstly, let $\tilde{L}: D \times U \to \mathbb{R}$ and C define the set of asymptotically stabilizing controllers for the nominal system $\tilde{f}_0(\cdot,\cdot)$ such that $x(\cdot)$ given by equation (3.18) satisfies $x(t) \to 0$ as $t \to \infty$ with $\tilde{f}(\cdot,\cdot) = \tilde{f}_0(\cdot,\cdot)$. Secondly, considering the controlled uncertain system define on equation (3.20) with performance functional from equation (3.19), and assuming $V: D \to \mathbb{R}, \tilde{\Gamma}: D \times U \to \mathbb{R}$ functions exist and a control law $\phi: D \to U$ where $V(\cdot)$ is a Lyapunov function such that

$$V(0) = 0 \qquad (3.21)$$

$$V(x) > 0, x \in D, \qquad x \neq 0 \qquad (3.22)$$

$$\phi(0) = 0 \quad (3.23)$$

$$V'^{(x)\tilde{f}(x,\phi(x))} \leq V'(x)\tilde{f}_0\big(x,\phi(x)\big) + \tilde{\Gamma}\big(x,\phi(x)\big), \qquad x \in D, \qquad \tilde{f}(\cdot,\cdot) \in \tilde{\mathcal{F}} \quad (3.24)$$

$$V'(x)\tilde{f}_0\big(x,\phi(x)\big) + \tilde{\Gamma}\big(x,\phi(x)\big) < 0, \qquad x \in D, \qquad x \neq 0 \quad (3.25)$$

$$H\big(x,\phi(x)\big) = 0, \qquad x \in D \quad (3.26)$$

$$H(x,u) \geq 0, \qquad x \in D, \qquad u \in U \quad (3.27)$$

where $H(\cdot,\cdot)$ is defined as

$$H(x,u) \triangleq \tilde{L}(x,u) + V'(x)\tilde{f}_0(x,u) + \tilde{\Gamma}(x,u) \quad (3.28)$$

If all the conditions stated above are to be satisfied (equations (3.21)-(3.27)), then there exists a neighborhood $D_0 \subset D$ of the origin such that if $x_0 \subset D_0$, the solution $x(t) = 0, t \geq 0$ of the controlled uncertain system is locally asymptotically stable or all $\tilde{f}(\cdot,\cdot) \in \tilde{\mathcal{F}}$. Furthermore, the performance functional on equation (3.19) can now be defined as

$$\tilde{J}_{\tilde{f}}\big(x_0,u(\cdot)\big) \triangleq \int_0^{\infty} \big[\tilde{L}\big(x(t),u(t)\big) + \tilde{\Gamma}\big(x(t),u(t)\big)\big]\,\big]\,dt \quad (3.29)$$

and, if $x_0 \subset D_0$, then the feedback control $u(t) = \phi\big(x(t)\big)$ minimizes the performance functional on equation (3.29). Going even further, if $D = \mathbb{R}^n, U = \mathbb{R}^m$ and $V(x) \to \infty$ as $\|x\| \to \infty$, then the solution $x(t) = 0, t \geq 0$ of the controlled uncertain system is globally asymptotically stable for all $\tilde{f}(\cdot,\cdot) \in \tilde{\mathcal{F}}$.

3.7 Robust feedback control of linear uncertain systems

Having defined the general case for all nonlinear uncertain systems, a better-suited formulation is used to deal with linear uncertain systems controlled by nonlinear controllers that minimize a polynomial cost function.

Firstly, the following linear uncertain system is considered

$$\dot{x}(t) = (A + \Delta A)x(t) + Bu(t), \qquad x(0) = 0, \qquad t \geq 0 \quad (3.30)$$

where the set of uncertain linear systems $\tilde{\mathcal{F}}$ is given by:

$$\{(A + \Delta A)x + Bu : x \in \mathbb{R}^n, A \in \mathbb{R}^{n\times n}, B \in \mathbb{R}^{n\times m}, \Delta A \in \Delta\} \quad (3.31)$$

And $\Delta \in \mathbb{R}^{n\times n}$ is a given bounded uncertainty set of the uncertain perturbation ΔA of the nominal system A. Secondly, for the linear uncertain system on equation (3.30), let the weighing matrices $R_1 \in \mathbb{P}^{n\times n}, R_2 \in \mathbb{P}^{m\times m}$ and $\hat{R}_k \in \mathbb{N}^{n\times n}, k = 2, \dots, r$, where r is a positive integer. Thirdly, it is assumed, there exists $\Omega: \mathbb{R}^{n\times n} \to \mathbb{R}^{n\times n}$ in such a way that

$$\Delta A^T P + P\Delta A \leq \Omega(P), \qquad \Delta \mathrm{A} \in \Delta, \qquad \mathrm{P} \in \mathbb{R}^{\mathrm{n}\times\mathrm{n}} \quad (3.32)$$

and there exists $\mathrm{P} \in \mathbb{P}^{n\times n}, M_k \in \mathbb{R}^{\mathrm{n}\times\mathrm{n}}, k = 2, \dots, r$ in such a manner that

$$0 = A^T P + PA + R_1 + \Omega(P) - PSP \quad (3.33)$$

$$0 = (A - SP)^T M_k + M_k(A - SP) + \hat{R}_k + \Omega(M_k) \quad (3.34)$$

where $S \triangleq BR_2^{-1}B^T$. Fourthly, let $\tilde{L}$ and $\tilde{\Gamma}$ be

$$\tilde{L}(x,u) = x^T \left(R_1 + \sum_{k=3}^{r} (x^T M_k x)^{k-1} \hat{R}_k + \left[\sum_{k=2}^{r} (x^T M_k x)^{k-1} M_k\right]^T S \left[\sum_{k=2}^{r} (x^T M_k x)^{k-1} M_k\right] \right) x + u^T R_2 u \quad (3.35)$$

$$\tilde{\Gamma}(x,u) = x^T \left(\Omega(P) + \sum_{k=2}^{r} (x^T M_k x)^{k-1} \Omega(M_k) \right) \quad (3.36)$$

Then, the linear uncertain system in equation (3.30) takes the performance functional

$$\tilde{J}_{\Delta A}\big(x_0, u(\cdot)\big) \triangleq \int_0^{\infty} \tilde{L}(x,u)\, dt \quad (3.37)$$

and is globally asymptotically stable for all $x_0 \in \mathbb{R}^n$ and $\Delta A \in \Delta$ with the feedback control

$$\phi(x) \triangleq -R_2^{-1}B^T \left[P + \sum_{k=2}^{r} (x^T M_k x)^{k-1} M_k \right] x \quad (3.38)$$

Next, it is necessary to assign an explicit structure to the set Δ and to the bounding function $\Omega(\cdot)$. For the uncertainty set Δ, it is assumed to be of the form

$$\Delta \triangleq \left\{ \Delta A \in \mathbb{R}^{n\times n}: \Delta \mathrm{A} = \sum_{i=1}^{p} \sigma_i A_i\,, \sum_{i=1}^{p} \frac{\sigma_i^2}{\alpha_i^2} \leq 1 \right\}, i = 1, \dots, p \quad (3.39)$$

where $A_i \in \mathbb{R}^{n\times n}$ are fixed matrices denoting the structure of the parametric uncertainty and σ_i is an uncertain real parameter that, for the linear dynamic system described in chapter 2 take the shape of

$$A_1 = \begin{bmatrix} 0 & 0 & 0 & 0 & 0 & 0 \\ 0 & 0 & 0 & 0 & 0 & 0 \\ 0 & 0 & 0 & 0 & 0 & 0 \\ 10 & 0 & 0 & 0 & 0 & 0 \\ 0 & 1 & 0 & 0 & 0 & 0 \\ 0 & 0 & -3 & 0 & 0 & 0 \end{bmatrix} \quad (3.40)$$

$$A_2 = \begin{bmatrix} 0 & 0 & 0 & 0 & 0 & 0 \\ 0 & 0 & 0 & 0 & 0 & 0 \\ 0 & 0 & 0 & 0 & 0 & 0 \\ 0 & -2 & 0 & 0 & 0 & 0 \\ 2 & 0 & 0 & 0 & 0 & 0 \\ 0 & 0 & 0 & 0 & 0 & 0 \end{bmatrix} \quad (3.41)$$

$$A_3 = \begin{bmatrix} 0 & 0 & 0 & 0 & 0 & 0 \\ 0 & 0 & 0 & 0 & 0 & 0 \\ 0 & 0 & 0 & 0 & 0 & 0 \\ 0 & 0 & 0 & 0 & 4 & 0 \\ 0 & 0 & 0 & -4 & 0 & 0 \\ 0 & 0 & 0 & 0 & 0 & 0 \end{bmatrix} \quad (3.42)$$

$$\sigma_1 = en^2 \cos M \quad (3.43)$$

$$\sigma_2 = en^2 \sin M \quad (3.44)$$

$$\sigma_3 = encos\, M \quad (3.45)$$

and α_i is an arbitrary positive scalar. For the bounding function $\Omega(\cdot)$, it takes the form

$$\Omega(\mathrm{P}) = \sum_{i=1}^{p} \left(\frac{\alpha_i^2}{\alpha}\right) A_i^T P A_i + \alpha P \quad (3.46)$$

where $\alpha = \sum_{i=1}^{p} \alpha_i$. Additionally, let

$$A_\alpha = A + \frac{\alpha}{2} I_n \quad (3.47)$$

where I_n denotes $n \times n$ identity matrices. For the present case study, $r = 2$ is enough to obtain the optimal robust controller and to solve the modified Riccati equations in (3.33)-(3.34). Therefore, equations (3.33)-(3-36) can be rewritten as

$$0 = {A_\alpha}^T P + P A_\alpha + R_1 + \sum_{i=1}^{p} \left(\frac{\alpha_i^2}{\alpha}\right) A_i^T P A_i - PSP \quad (3.48)$$

$$0 = (A_\alpha - SP)^T M_2 + M_2(A_\alpha - SP) + \hat{R}_2 + \sum_{i=1}^{p} \left(\frac{\alpha_i^2}{\alpha}\right) A_i^T M_2 A_i \quad (3.49)$$

$$\tilde{L}(x,u) = x^T\left(R_1 + x^T M_2 x \hat{R}_2 + (x^T M_2 x)^2 M_2 S M_2\right)x + u^T R_2 u \quad (3.50)$$

$$\tilde{\Gamma}(x,u) = x^T\left(\sum_{i=1}^{p}\left(\frac{\alpha_i^2}{\alpha}\right)A_i^T P A_i + \alpha P + x^T M_2 x\left[\sum_{i=1}^{p}\left(\frac{\alpha_i^2}{\alpha}\right)A_i^T M_2 A_i + \alpha M_2\right]\right)x \quad (3.51)$$

The control matrices R_1 and R_2 can also be written using the modified Bryson's Method, in which they take the following shape

$$R_1 = \begin{bmatrix} \frac{\eta_1}{x_{1\,max}^2} & 0 & \cdots & 0 \\ 0 & \frac{\eta_2}{x_{1\,max}^2} & \cdots & 0 \\ \vdots & \vdots & \ddots & \vdots \\ 0 & 0 & \cdots & \frac{\eta_n}{x_{n\,max}^2} \end{bmatrix} \quad (3.52)$$

where $\eta_1,\ \eta_2,\ \ldots,\ \eta_n \geq 1$ and $x_{1\,max},\ x_{2\,max}, \ldots, x_{n\,max}$ are maximum acceptable values for each state, which, in the rendezvous problem, is the initial state since the relative distance between the two spacecrafts is greater than in any other state, and

$$R_2 = \begin{bmatrix} \frac{\lambda_1}{u_{1\,max}^2} & 0 & \cdots & 0 \\ 0 & \frac{\lambda_2}{u_{1\,max}^2} & \cdots & 0 \\ \vdots & \vdots & \ddots & \vdots \\ 0 & 0 & \cdots & \frac{\lambda_n}{u_{n\,max}^2} \end{bmatrix} \quad (3.53)$$

where $0 < \lambda_1,\ \lambda_2,\ \ldots,\ \lambda_n \leq 1$ and $u_{1\,max},\ u_{2\,max}, \ldots, u_{n\,max}$ are maximum acceptable values for each control, which, for the current problem, is the maximum thrust force generated in each axis. Matrix $\hat{R}_2$ is also a diagonal matrix with the following shape

$$\hat{R}_2 = \begin{bmatrix} \varepsilon_1 & 0 & \cdots & 0 \\ 0 & \varepsilon_2 & \cdots & 0 \\ \vdots & \vdots & \ddots & \vdots \\ 0 & 0 & \cdots & \varepsilon_n \end{bmatrix} \quad (3.54)$$

where $\varepsilon_1,\ \varepsilon_2,\ \ldots,\ \varepsilon_n \geq 0$. Because the numerator on each matrix (η_n, λ_n and ε_n) has a great effect on the performance and robustness of the controller, many iterations and tests were conducted to find the best-suited values for each one.

Chapter 4 – Simulation Results and Discussion

In this chapter, four examples will be presented to demonstrate and validate the effectiveness and robustness of the nonlinear controller when applied to a linear uncertain system. Although all four cases use the same target orbit and only the initial state is changed to evaluate the performance for a wide range of distances, only the last one will take into account the uncertainty as a perturbation while simulating the linear system. Also, for those simulations, to generate data and process it, the programming language *Python™* is used.

Firstly, a table is presented with the necessary target orbit parameters and some spacecraft properties (thrust and vehicle mass) needed to generate a linear dynamic system that describes the rendezvous process accurately. Secondly, the linear dynamic system is discretized in order to solve the rendezvous problem to the target orbit. Further on this chapter, two methods are described to understand how all the matrices mentioned in the previous chapters are obtained. Lastly, a detailed analysis is made to fully understand and evaluate the controller's performance.

4.1 Target orbit parameters and spacecraft properties

Nowadays, most RND operations are performed to deliver personnel and supplies to the ISS. Based on this data and because the ISS has a near-circular orbit, it is appropriate to study the controller performance using its orbital parameters as the target orbit. Having only the perigee distance and the eccentricity of the target orbit, all the other parameters must be calculated using the following equations:

$$r_a = r_p \times \frac{1+e}{1-e} \quad (4.1)$$

$$a = \frac{r_p + r_a}{2} \quad (4.2)$$

$$T = 2\pi\sqrt{a^3/\mu} \quad (4.3)$$

$$n = \frac{2\pi}{T} \quad (4.4)$$

$$tp = 2\pi\sqrt{\frac{{r_a}^3}{\mu}} \quad (4.5)$$

$$M = n * tp \quad (4.6)$$

Table 4.1: Target orbit parameters

Parameter	*Value*
r_p *[m]*	6728140
e	0.01
r_a *[m]*	6864062
a [m]	6796101
μ [$m^3.s^{-2}$]	3.986 x 1014
T [s]	5575.7
n [rad/s]	0.00113
tp [s]	5659.5
M [rad]	6.378

Another important parameter is the chaser spacecraft's mass that is needed to generate the control matrix B. Furthermore, a saturation function is employed to limit the maximum thrust force generated on each axis by the chaser spacecraft so that the simulation portrays a real engineering problem as accurately as possible. Both mass and maximum thrust forces on each axis were chosen based on multiple articles that simulate similar cases such as Wan et al. [11] and Miele et al. [4].

Table 4.2: Chaser Spacecraft characteristics

Parameter	*Value*
m [kg]	200
Maximum control thrust along x-axis [N]	100
Maximum control thrust along y-axis [N]	100
Maximum control thrust along z-axis [N]	20

4.2 Linear Dynamic system

The next step to start the simulation is to generate the linear dynamic system that portrays the orbital rendezvous, combining matrices $A, \Delta A$ and B from chapter 2 with the orbital elements and the chase spacecraft characteristic above. Because the target orbit will suffer no change, all the above matrices are constant for all three examples. The following results were obtained:

$$A = \begin{bmatrix} 0 & 0 & 0 & 1.000 \cdot 10^{0} & 0 & 0 \\ 0 & 0 & 0 & 0 & 1.000 \cdot 10^{0} & 0 \\ 0 & 0 & 0 & 0 & 0 & 1.000 \cdot 10^{0} \\ 3.810 \cdot 10^{-6} & 0 & 0 & 0 & 2.254 \cdot 10^{-3} & 0 \\ 0 & 0 & 0 & -2.254 \cdot 10^{-3} & 0 & 0 \\ 0 & 0 & -1.270 \cdot 10^{-6} & 0 & 0 & 0 \end{bmatrix} \quad (4.7)$$

$$B = \begin{bmatrix} 0 & 0 & 0 \\ 0 & 0 & 0 \\ 0 & 0 & 0 \\ 0.005 & 0 & 0 \\ 0 & 0.005 & 0 \\ 0 & 0 & 0.005 \end{bmatrix} \quad (4.8)$$

$$\Delta A = \begin{bmatrix} 0 & 0 & 0 & 0 & 0 & 0 \\ 0 & 0 & 0 & 0 & 0 & 0 \\ 0 & 0 & 0 & 0 & 0 & 0 \\ 1.264 \cdot 10^{-7} & -2.396 \cdot 10^{-9} & 0 & 0 & 4.487 \cdot 10^{-5} & 0 \\ 2.396 \cdot 10^{-9} & 1.264 \cdot 10^{-8} & 0 & -4.487 \cdot 10^{-5} & 0 & 0 \\ 0 & 0 & -3.793 \cdot 10^{-8} & 0 & 0 & 0 \end{bmatrix} \quad (4.9)$$

and the state matrix, A, can be added up to the norm-bounded matrix, ΔA,

$$A + \Delta A = \begin{bmatrix} 0 & 0 & 0 & 1.000 \cdot 10^{0} & 0 & 0 \\ 0 & 0 & 0 & 0 & 1.000 \cdot 10^{0} & 0 \\ 0 & 0 & 0 & 0 & 0 & 1.000 \cdot 10^{0} \\ 3.936 \cdot 10^{-6} & -2.396 \cdot 10^{-9} & 0 & 0 & 2.299 \cdot 10^{-3} & 0 \\ 2.396 \cdot 10^{-9} & 1.264 \cdot 10^{-8} & 0 & -2.299 \cdot 10^{-3} & 0 & 0 \\ 0 & 0 & -1.308 \cdot 10^{-6} & 0 & 0 & 0 \end{bmatrix} \quad (4.10)$$

Regarding the output vector $y(t)$ from equation (3.5), matrix C is an output matrix related to the measurability of the state variables and it takes the shape

$$C = \begin{bmatrix} 1 & 0 & 0 & 0 & 0 & 0 \\ 0 & 1 & 0 & 0 & 0 & 0 \\ 0 & 0 & 1 & 0 & 0 & 0 \end{bmatrix} \quad (4.11)$$

Furthermore, $\forall_i, \sigma_i$ are also constant because they only depend on the target orbit, hence, they can be quickly obtained:

$$\sigma_1 = 1.264 \cdot 10^{-8} \quad (4.12)$$
$$\sigma_2 = 1.198 \cdot 10^{-9} \quad (4.13)$$
$$\sigma_3 = 1.122 \cdot 10^{-5} \quad (4.14)$$

As for the arbitrary positive scalars, α_i, many iterations were performed to achieve the best results for the control while taking into consideration the condition:

$$\sum_{i=1}^{p} \frac{\sigma_i^2}{\alpha_i^2} \leq 1 \, , i = 1, \dots, p \quad (4.15)$$

Thus, the best results obtained were achieved by using:

$$\alpha_1 = 2.4 \cdot 10^{-4} \quad (4.16)$$
$$\alpha_2 = 1.4 \cdot 10^{-3} \quad (4.17)$$
$$\alpha_3 = 1.3 \cdot 10^{-3} \quad (4.18)$$

$$\alpha = \sum_{i=1}^{p} \alpha_i = \alpha_1 + \alpha_2 + \alpha_3 = 2.94 \cdot 10^{-3} \quad (4.19)$$

Having all the above parameters defined, A_α can now be determined using equation (3.47):

$$A_\alpha = \begin{bmatrix} 1.470 \cdot 10^{-3} & 0 & 0 & 1.000 \cdot 10^{0} & 0 & 0 \\ 0 & 1.470 \cdot 10^{-3} & 0 & 0 & 1.000 \cdot 10^{0} & 0 \\ 0 & 0 & 1.470 \cdot 10^{-3} & 0 & 0 & 1.000 \cdot 10^{0} \\ 3.810 \cdot 10^{-6} & 0 & 0 & 1.470 \cdot 10^{-3} & 2.254 \cdot 10^{-3} & 0 \\ 0 & 0 & 0 & -2.254 \cdot 10^{-3} & 1.470 \cdot 10^{-3} & 0 \\ 0 & 0 & -1.270 \cdot 10^{-6} & 0 & 0 & 1.470 \cdot 10^{-3} \end{bmatrix} \quad (4.20)$$

In order to generate trajectory, velocity and thrust force data for the linear dynamic system, a model must be used to solve them. For the present case study and considering the continuous-time state equations (3.4) and (3.5), a solution must be found where it is excited by the initial state $x(0)$ and the input $u(t)$. This solution can be obtained by pre-multiplying e^{-At} on both sides of equation (3.4) yielding

$$e^{-At}\dot{x}(t) - e^{-At}Ax(t) = e^{-At}Bu(t) \quad (4.21)$$

which implies

$$\frac{d}{dt}\left(e^{-At}x(t)\right) = e^{-At}Bu(t) \quad (4.22)$$

and integrating from 0 to t

$$\left(e^{-At}x(\tau)\right)\Big|_{\tau=0}^{t} = \int_0^t e^{-A\tau}Bu(\tau)\ d\tau \quad (4.23)$$

the following equation is obtained

$$e^{-At}x(t) - e^{0}x(0) = \int_0^t e^{-A\tau}Bu(\tau)\ d\tau \quad (4.24)$$

Because the inverse of e^{-At} is e^{At} and $e^{0} = I$ and reordering equation (4.24) the final solution is obtained

$$x(t) = e^{At}x(0) + \int_0^t e^{A(t-\tau)}Bu(\tau)\ d\tau \quad (4.25)$$

Although equation (4.25) provides a solution, it still cannot be solved on a computer. To solve this problem a discretization is used in order to compute the linear system. Firstly, let $u(t)$ be an input generated by a computer and let

$$u(t) = u(kT) =: u[k], \qquad for\ kT \leq t < (k+1)T \quad (4.26)$$

for $k = 0, 1, 2, \dots$. Since this input changes values only at discrete-time instants, and computing (4.25) at $t = kT$ and $t = (k+1)T$ yields

$$x[k] = x(kT) = e^{AkT}x(0) + \int_0^{kT} e^{A(kT-\tau)}Bu(\tau)\ d\tau \quad (4.27)$$

$$x[k+1] = x((k+1)T) = e^{A(k+1)T}x(0) + \int_0^{(k+1)T} e^{A((k+1)T-\tau)}Bu(\tau)\ d\tau \quad (4.28)$$

Equation (4.28) can be rewritten as

$$x[k+1] = e^{AT}\left[e^{AkT}x(0) + \int_0^{kT} e^{A(kT-\tau)}Bu(\tau)\ d\tau\right] + \int_{kT}^{(k+1)T} e^{A(kT+T-\tau)}Bu(\tau)\ d\tau \quad (4.29)$$

and by introducing a new variable $\alpha = kT + T - \tau$

$$x[k+1] = e^{AT}x[k] + \left(\int_0^T e^{A\alpha}\ d\alpha\right)Bu[k] \quad (4.30)$$

In a more friendly way, and if an input changes value only at discrete-time instants kT and only computing the responses at $t = kT$, equation (4.30) can be written as

$$x[k+1] = A_d x[k] + B_d u[k] \quad (4.31)$$

where

$$A_d = e^{AT} \quad (4.32)$$

$$B_d = \left(\int_0^T e^{A\tau}\ d\tau\right)B \quad (4.33)$$

The only step left is to calculate these two matrices using power series, using the following equations

$$A_d = I + \frac{AT}{1!} + \frac{A^2T^2}{2!} + \cdots + \frac{A^nT^n}{n!} \quad (4.34)$$

$$B_d = \left(IT + \frac{AT^2}{2!} + \frac{A^2T^3}{3!} + \cdots + \frac{A^nT^{n+1}}{(n+1)!}\right)B \quad (4.35)$$

Parameter n will directly affect how accurate these two matrices will be, which, based on the available literature, $n = 3$ is enough to get accurate results. Also, because matrices A and B are constant throughout each simulation, and since A_d and B_d only depend on those same matrices and the time step, T, which is constant too, they're also constant for the first three examples. For the fourth case, because the norm-bounded matrix ΔA is considered a perturbation to the system, matrix A_d will present different values. Thus, for the first three cases, the discretized matrices are as follows

$$A_d = \begin{bmatrix} 1.000 \cdot 10^{0} & 0 & 0 & 1.000 \cdot 10^{-2} & 1.129 \cdot 10^{-7} & 0 \\ -1.431 \cdot 10^{-15} & 1.000 \cdot 10^{0} & 0 & -1.129 \cdot 10^{-7} & 1.000 \cdot 10^{-2} & 0 \\ 0 & 0 & 1.000 \cdot 10^{0} & 0 & 0 & 1.000 \cdot 10^{-2} \\ 3.810 \cdot 10^{-8} & 0 & 0 & 1.000 \cdot 10^{0} & 2.254 \cdot 10^{-5} & 0 \\ -4.293 \cdot 10^{-1} & 0 & 0 & -2.254 \cdot 10^{-5} & 1.000 \cdot 10^{0} & 0 \\ 0 & 0 & -1.270 \cdot 10^{-8} & 0 & 0 & 1.000 \cdot 10^{0} \end{bmatrix} \quad (4.36)$$

$$B_d = \begin{bmatrix} 2.500 \cdot 10^{-7} & 1.878 \cdot 10^{-12} & 0 \\ -1.878 \cdot 10^{-12} & 2.500 \cdot 10^{-7} & 0 \\ 0 & 0 & 2.500 \cdot 10^{-7} \\ 5.000 \cdot 10^{-5} & 5.634 \cdot 10^{-10} & 0 \\ -5.634 \cdot 10^{-10} & 5.000 \cdot 10^{-5} & 0 \\ 0 & 0 & 5.000 \cdot 10^{-5} \end{bmatrix} \quad (4.37)$$

4.3 Preliminary system analysis

Since the linear dynamic system is defined, with matrices $A, \Delta A, B,$ and C, it can be tested to evaluate the system's controllability and observability to understand whether the chosen linear system can be observed and controlled or not. Regarding the observability matrix, $\mathcal{O}$, using equation (3.7), and calculating its rank the following result was obtained

$$rank(\mathcal{O}) = 6 \quad (4.38)$$

As for the controllability matrix, $\mathcal{C}$, using equation (3.8), and calculating its rank, the subsequent result was achieved

$$rank(\mathcal{C}) = 6 \quad (4.39)$$

Because both matrices are enormous (dimensions 12×6), only the rank is presented since it is the only value needed to evaluate the controllability and observability of the system. Now, looking at the dimensions of matrices $A, B,$ and C, $n = 6$, therefore, $rank(\mathcal{C}) = n$ and $rank(\mathcal{O}) = n$ coming to the conclusion that the selected linear dynamic system is both controllable and observable.

4.4 Modified Riccati equations

To calculate the control law for the nonlinear controller, matrices P and M_2 need to be determined first. To do so, the modified Riccati equations (3.48)-(3.49) were used. Since those equations cannot be solved using the *CARE* (continuous algebraic Riccati equation) function on *Python™*, they were transformed into differential equations so they can be solved using the Euler's method:

$$\dot{P} = {A_\alpha}^T P + P A_\alpha + R_1 + \sum_{i=1}^{p} \left(\frac{\alpha_i^2}{\alpha}\right) A_i^T P A_i - PSP \quad (4.40)$$

$$\dot{M}_2 = (A_\alpha - SP)^T M_2 + M_2 (A_\alpha - SP) + \hat{R}_2 + \sum_{i=1}^{p} \left(\frac{\alpha_i^2}{\alpha}\right) A_i^T M_2 A_i \quad (4.41)$$

This numerical method is implemented to solve ODE (ordinary differential equations) with a given initial value, i.e., having an unknown curve that starts at the given initial point, $y(t_0) = y_0$, and satisfies a given differential equation, $y'(t) = f(t, y(t))$, and using a small step, h, along the tangent line described by that same differential equation, a new point of the unknown curve can be approximated using:

$$y_{n+1} = y_n + hf(t_n, y_n) \quad (4.42)$$

This process can be repeated to accurately describe the unknown curve.
On the present case study, the Euler's method is used not to find the unknown curve but to find the point on that curve where the two differential equations are equal to zero:

$$\dot{P} = 0 \quad (4.43)$$
$$\dot{M}_2 = 0 \quad (4.44)$$

Because it would take too much time and resources to find an absolute zero on both equations, another condition was created to deal with this problem. If $y_{n+1} - y_n \leq 10^{-3}$, then the program will stop and y_{n+1} will provide accurate values for matrices P and M_2.
Since the Euler's method is only used to find the point where the differential equations are zero, the step size needs to be small enough to "catch" this point but, at the same time, not

too small, considering that the processing time will increase greatly with smaller h. Consequently, for all the three case studies, $h = 0.01$ was used. The only thing left to be defined is the given initial point, $y(t_0) = y_0$, i.e., give initial estimations to P and M_2 on the first iteration. Thus, both matrices start the process as $P_0 = I_6$ and $M_{2_0} = I_6$.

4.5 Case studies

In this section, four different case studies are presented in order to analyze and compare each other, taking into account trajectory robustness and control effectiveness. The first three examples will only simulate the linear system with no perturbations, i.e. the norm-bounded matrix ΔA is not used to model the solutions of the ODE, while the fourth example will take into account the uncertainty parameter as a perturbation. In this simulation, based on the available literature, a time step of 0.01 seconds was used to obtain all the data. For the four cases, trajectory, relative position, and generated thrust will be presented. Velocity data will be presented in the annex since it is not of great relevance to the current analysis.

4.5.1 First example

For the first example, the initial state is

$$x_0 = \begin{bmatrix} 3000 \\ -4000 \\ 20 \\ -3 \\ 4 \\ -0.02 \end{bmatrix}, \quad (4.45)$$

and using the modified Bryson's method, matrices R_1 and R_2 can be created, obtaining

$$R_1 = \begin{bmatrix} \frac{10^5}{3000^2} & 0 & 0 & 0 & 0 & 0 \\ 0 & \frac{10^5}{(-4000)^2} & 0 & 0 & 0 & 0 \\ 0 & 0 & \frac{10^0}{20^2} & 0 & 0 & 9 \\ 0 & 0 & 0 & \frac{10^4}{(-3)^2} & 0 & 0 \\ 0 & 0 & 0 & 0 & \frac{10^4}{4^2} & 0 \\ 0 & 0 & 0 & 0 & 0 & \frac{10^0}{(-0.02)^2} \end{bmatrix}, \quad (4.46)$$

$$R_2 = \begin{bmatrix} \frac{0.5}{100^2} & 0 & 0 \\ 0 & \frac{0.5}{100^2} & 0 \\ 0 & 0 & \frac{1}{20^2} \end{bmatrix}, \quad (4.47)$$

Regarding matrix $\hat{R}_2$, through trial and error and considering the smoothness of the trajectory and the robustness of the controller, the following result was obtained

$$\hat{R}_2 = \begin{bmatrix} 10^{-2} & 0 & 0 & 0 & 0 & 0 \\ 0 & 10^{-2} & 0 & 0 & 0 & 0 \\ 0 & 0 & 10^{-2} & 0 & 0 & 9 \\ 0 & 0 & 0 & 1.1 \cdot 10^{3} & 0 & 0 \\ 0 & 0 & 0 & 0 & 10^{3} & 0 \\ 0 & 0 & 0 & 0 & 0 & 10^{2} \end{bmatrix}, \quad (4.48)$$

With matrices R_1, R_2 and $\hat{R}_2$ calculated, Euler's method can now be applied to estimate matrices P and M_2. Using a step of $h = 0.01$ the resulting matrices were obtained

$$P = \begin{bmatrix} 1.319 \cdot 10^{1} & -7.000 \cdot 10^{-5} & 0 & 5.593 \cdot 10^{-1} & 6.000 \cdot 10^{-5} & 0 \\ -7.000 \cdot 10^{-5} & 8.502 & 0 & -6.000 \cdot 10^{-5} & 4.803 \cdot 10^{-1} & 0 \\ 0 & 0 & 8.491 & 0 & 0 & 1.694 \\ 5.593 \cdot 10^{-1} & -6.000 \cdot 10^{-5} & 0 & 4.717 \cdot 10^{1} & 6.400 \cdot 10^{-4} & 0 \\ 6.000 \cdot 10^{-5} & 4.803 \cdot 10^{-1} & 0 & 6.400 \cdot 10^{-4} & 3.540 \cdot 10^{1} & 0 \\ 0 & 0 & 1.694 & 0 & 0 & 5.005 \cdot 10^{2} \end{bmatrix}, \quad (4.49)$$

$$M_2 = \begin{bmatrix} 1.134 \cdot 10^{1} & 3.000 \cdot 10^{-5} & 0 & 2.034 \cdot 10^{-1} & -1.000 \cdot 10^{-5} & 0 \\ 3.000 \cdot 10^{-5} & 9.233 & 0 & 2.000 \cdot 10^{-5} & 1.380 \cdot 10^{-1} & 0 \\ 0 & 0 & 1.627 & 0 & 0 & 2.911 \cdot 10^{-1} \\ 2.034 \cdot 10^{-1} & 2.000 \cdot 10^{-5} & 0 & 2.333 \cdot 10^{1} & 6.700 \cdot 10^{-4} & 0 \\ -1.000 \cdot 10^{-5} & 1.380 \cdot 10^{-1} & 0 & -6.700 \cdot 10^{-4} & 2.827 \cdot 10^{1} & 0 \\ 0 & 0 & 2.911 \cdot 10^{-1} & 0 & 0 & 1.051 \cdot 10^{2} \end{bmatrix}, \quad (4.50)$$

Now, the linear dynamic system can be simulated using the matrix exponential method. The nonlinear controller will stop its action course when the rendezvous is accomplished, that is when the state vector is equal to 0. Fig. 4.1 shows the rendezvous trajectory\y described by the chaser spacecraft until it achieves the rendezvous task.

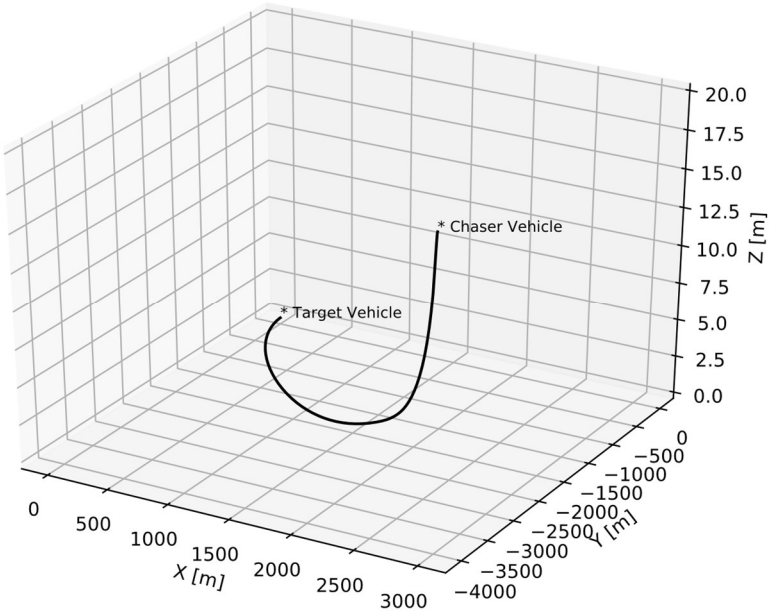

Figure 4.1: Rendezvous trajectory of the chaser spacecraft for the initial state $x_0 = [3000 \quad -4000 \quad 20 \quad -3 \quad 4 \quad -0.02]^T$.

This trajectory presents a smooth profile with no abrupt turns. It is also noticeable that the controller firstly tries to converge the z-axis to zero and, then, almost at the same rate, the x-

axis and the y-axis. From figs 4.2-4.3, displaying the 3 axes with respect to time, the zero solution to the linear dynamic system is indeed asymptotically stable and it is also noticeable that until $t = 600\,s$ the controller employs a high rate of convergence until it reaches short relative distances in which it changes this rate to make sure there is no overshooting the target. For the z-axis, the same thing happens but for a shorter period (around $t = 200\,s$)

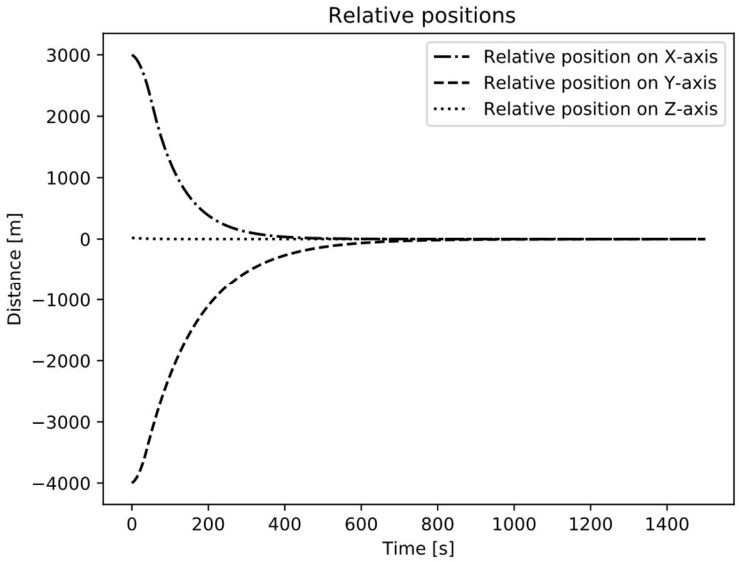

Figure 4.2: Relative position on each axis for the initial state $x_0 = [3000 \quad -4000 \quad 20 \quad -3 \quad 4 \quad -0.02]^T$.

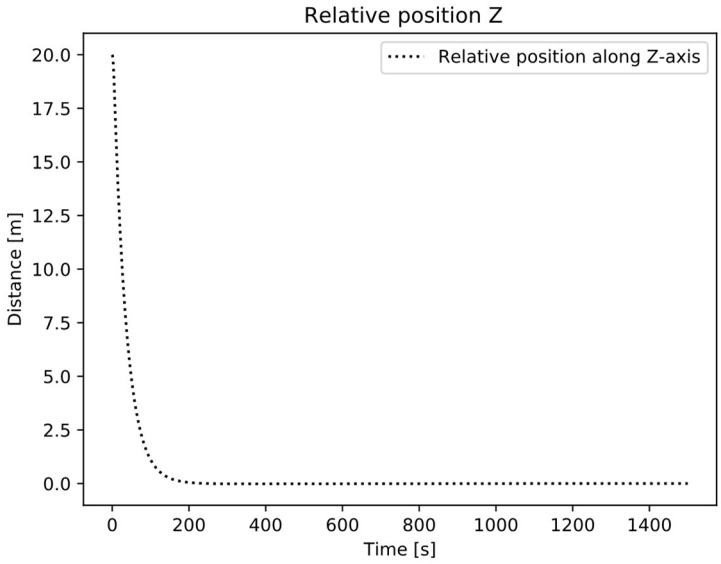

Figure 4.3: Relative position on the z-axis for the initial state $x_0 = [3000 \quad -4000 \quad 20 \quad -3 \quad 4 \quad -0.02]^T$.

Next, Fig 4.4 reveals the thrust profile for every axis. Because a saturation function was used, the maximum thrust on each axis is limited to the displayed values, also mentioned on the spacecraft properties. At first, the thrust profile appears to be a solid rectangle, but is, in fact, a single line with a bang-bang profile applied by the control, as can be shown on (d), (e) and (f).

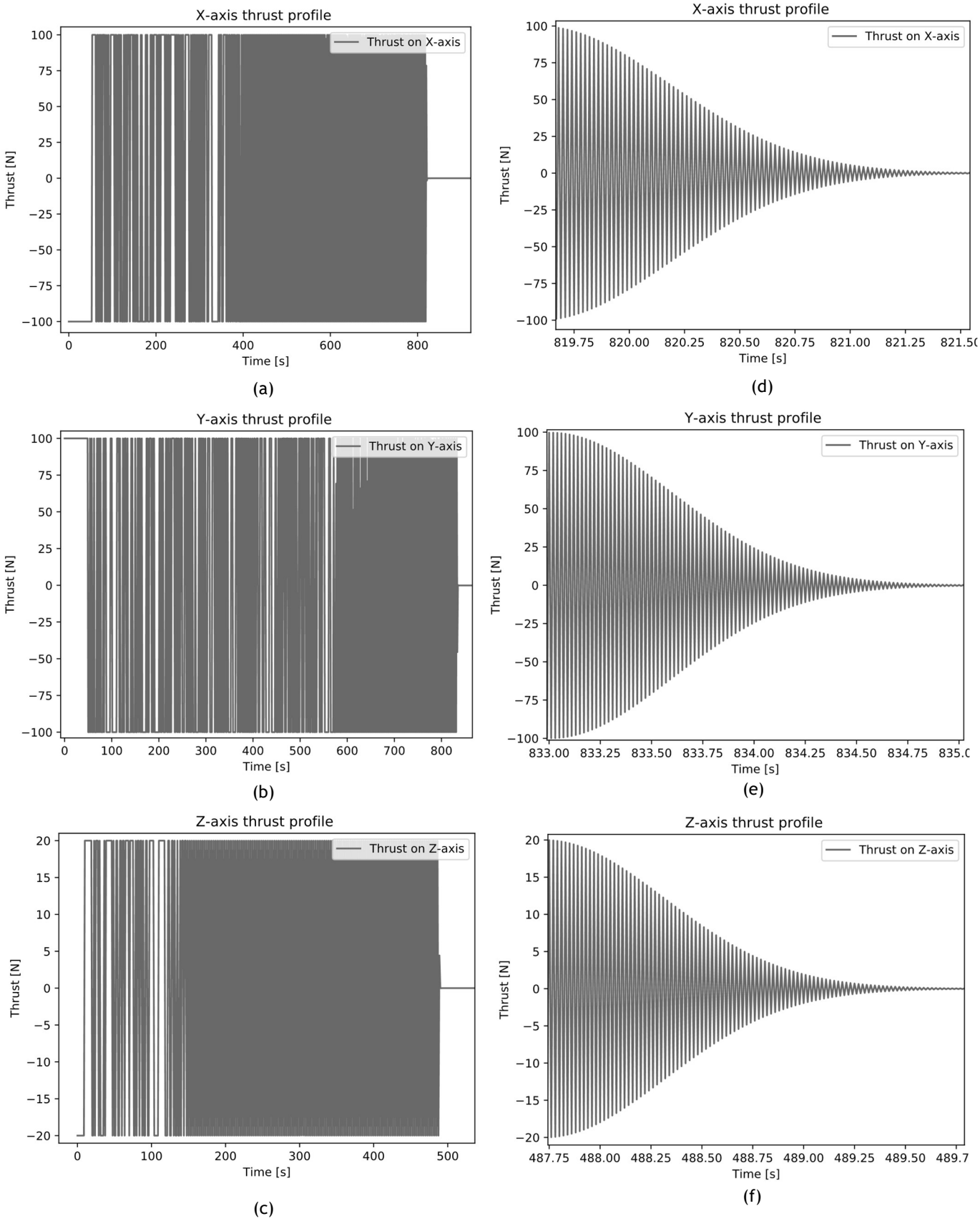

Figure 4.4: Thrust profile for each axis (a, b, c) and a closer look at the bang-bang profile (d, e, f) for the initial state $x_0 = [3000 \quad -4000 \quad 20 \quad -3 \quad 4 \quad -0.02]^T$.

It is also possible to observe when the controller stops its action course by noticing how the line flattens out and the thrust force produced is equal to zero Newtons. Furthermore, as stated before, the z-axis is the first to converge asymptotically to zero since the thrust produced on this axis stops at around 500 seconds while the other two axes stay active until around 850 seconds.

4.5.2 Second example

In the next example, both initial positions and velocities are increased by one order of magnitude to test the controller robustness and effectiveness when dealing with high relative distances and velocities. Therefore, the initial state can be written as follows

$$x_0 = \begin{bmatrix} 30000 \\ -40000 \\ 200 \\ -30 \\ 40 \\ -0.2 \end{bmatrix} \quad (4.51)$$

and matrices R_1 and R_2 can be created, using modified Bryson's method

$$R_1 = \begin{bmatrix} \frac{10^2}{30000^2} & 0 & 0 & 0 & 0 & 0 \\ 0 & \frac{10^2}{(-40000)^2} & 0 & 0 & 0 & 0 \\ 0 & 0 & \frac{10^0}{200^2} & 0 & 0 & 9 \\ 0 & 0 & 0 & \frac{10^4}{(-30)^2} & 0 & 0 \\ 0 & 0 & 0 & 0 & \frac{10^6}{40^2} & 0 \\ 0 & 0 & 0 & 0 & 0 & \frac{10^0}{(-0.2)^2} \end{bmatrix} \quad (4.52)$$

$$R_2 = \begin{bmatrix} \frac{0.1}{100^2} & 0 & 0 \\ 0 & \frac{0.1}{100^2} & 0 \\ 0 & 0 & \frac{1}{20^2} \end{bmatrix} \quad (4.53)$$

Just as in the first example, matrix $\hat{R}_2$ is created using trial and error while taking into account the controller robustness. Thus, the matrix that presents the best results for the given initial state in (4.51) is

$$\hat{R}_2 = \begin{bmatrix} 10^{-2} & 0 & 0 & 0 & 0 & 0 \\ 0 & 10^{-2} & 0 & 0 & 0 & 0 \\ 0 & 0 & 10^{-2} & 0 & 0 & 9 \\ 0 & 0 & 0 & 1.1 \cdot 10^3 & 0 & 0 \\ 0 & 0 & 0 & 0 & 10^4 & 0 \\ 0 & 0 & 0 & 0 & 0 & 10^2 \end{bmatrix} \quad (4.54)$$

Once again, Euler's method is implemented to solve the modified Riccati equations and find matrices P and M_2 using the same step, h, as the previous example.

$$P = \begin{bmatrix} 7.484 \cdot 10^{-1} & 3.000 \cdot 10^{-5} & 0 & 1.394 \cdot 10^{-1} & 1.000 \cdot 10^{-5} & 0 \\ 3.000 \cdot 10^{-5} & 1.634 & 0 & 0 & 4.139 \cdot 10^{-2} & 0 \\ 0 & 0 & 8.491 & 0 & 0 & 1.063 \\ 1.394 \cdot 10^{-1} & 0 & 0 & 2.149 & -6.900 \cdot 10^{-4} & 0 \\ 1.000 \cdot 10^{-5} & 4.139 \cdot 10^{-2} & 0 & -6.900 \cdot 10^{-4} & 1.581 \cdot 10^{1} & 0 \\ 0 & 0 & 1.694 & 0 & 0 & 5.223 \cdot 10^{1} \end{bmatrix} \quad (4.55)$$

$$M_2 = \begin{bmatrix} 4.094 \cdot 10^{1} & 7.900 \cdot 10^{-4} & 0 & 9.567 \cdot 10^{-1} & -7.000 \cdot 10^{-5} & 0 \\ 7.900 \cdot 10^{-4} & 2.962 \cdot 10^{1} & 0 & -7.000 \cdot 10^{-5} & 4.181 \cdot 10^{-1} & 0 \\ 0 & 0 & 1.827 & 0 & 0 & 1.492 \\ 9.597 \cdot 10^{-1} & -7.000 \cdot 10^{-5} & 0 & 1.027 \cdot 10^{2} & 7.550 \cdot 10^{-3} & 0 \\ -7.000 \cdot 10^{-5} & 4.181 \cdot 10^{-1} & 0 & 7.550 \cdot 10^{-3} & 1.265 \cdot 10^{2} & 0 \\ 0 & 0 & 1.492 & 0 & 0 & 9.886 \cdot 10^{1} \end{bmatrix} \quad (4.56)$$

The resulting rendezvous trajectory for the second example, using the matrix exponential to simulate the linear system as a function of time is portrayed in fig 4.5.

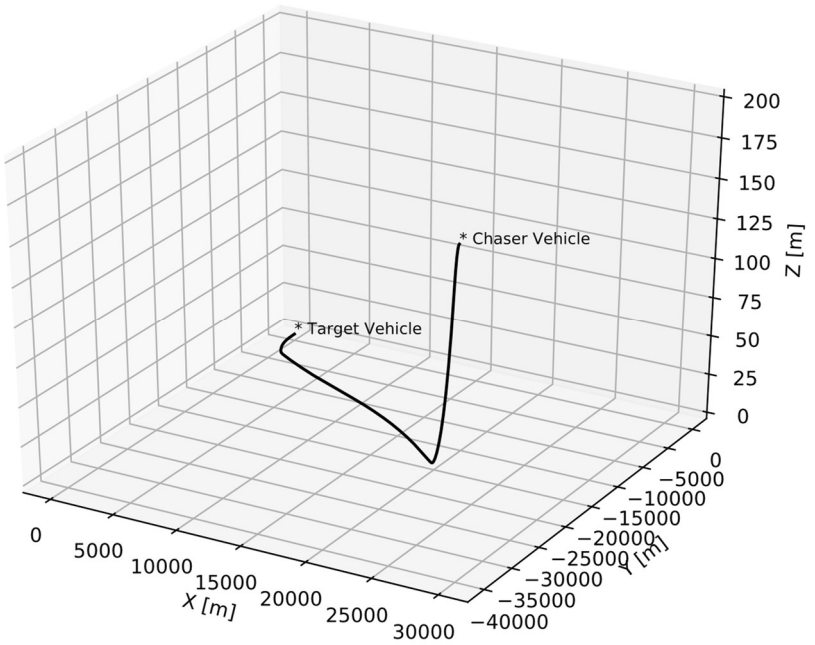

Figure 4.5: Rendezvous trajectory of the chaser spacecraft for the initial state $x_0 = [30000 \quad -40000 \quad 200 \quad -30 \quad 40 \quad -0.02]^T$.

Like the first example, this trajectory shows a smooth profile, with no overshooting. Because the relative distances are greater on the x and y-axis, the controller now applies a high rate of convergence until $t = 1000\ s$, where it switches to a lower one after that to avoid overshooting. For the z-axis, this phenomenon occurs until $t = 500\ s$. Additionally, the controller firstly converges the z-axis to zero and then, the x-axis and y-axis approach zero almost at the same rate. A few seconds before the final stage of the rendezvous, the x-axis approaches zero prior to the y-axis. A more detailed view of this complex process is presented in figs 4.6-4.7.

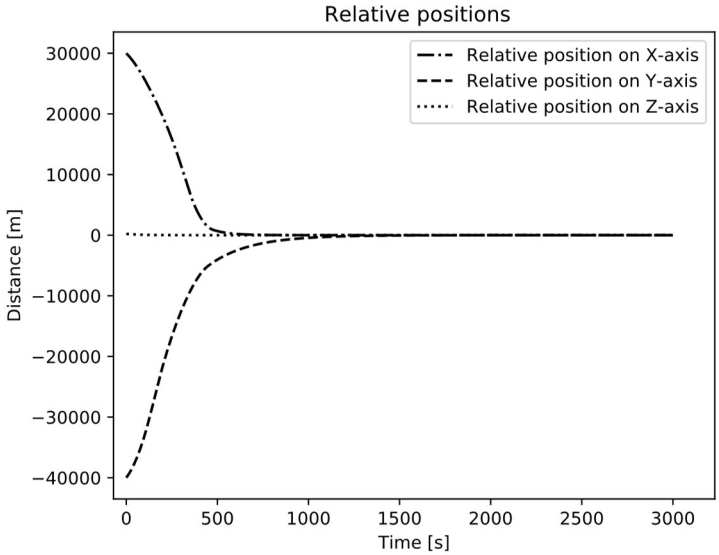

Figure 4.6: Relative position on each axis for the initial state state $x_0 = [30000 \quad -40000 \quad 200 \quad -30 \quad 40 \quad -0.02]^T$.

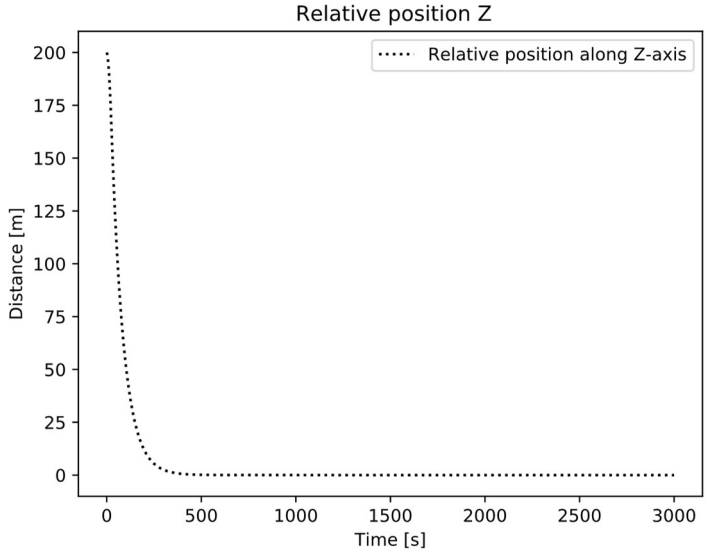

Figure 4.7: Relative position on the z-axis for the initial state state $x_0 = [30000 \quad -40000 \quad 200 \quad -30 \quad 40 \quad -0.02]^T$.

Regarding the thrust analysis of the second example, fig 4.8 reveals that contrarily to the first example, the thrust generated on the x-axis stays at -100 N for almost 400 seconds, changing to 100 N for the next 100 seconds. This variation on the thrust signal reveals that its vector sense has changed. After 500 seconds, the controller, once again, generates a bang-bang profile to converge the solution to zero. On the y-axis, something similar happens. In the first 150 seconds, the controller generates 100 N, which changes to -100 N until around 500 seconds, showing, yet again, that the thrust vector switches its sense. Afterward, the bang-bang profile is exhibited until the solution $x = 0$ is found. Only the z-axis presents the same behavior as in the first example.

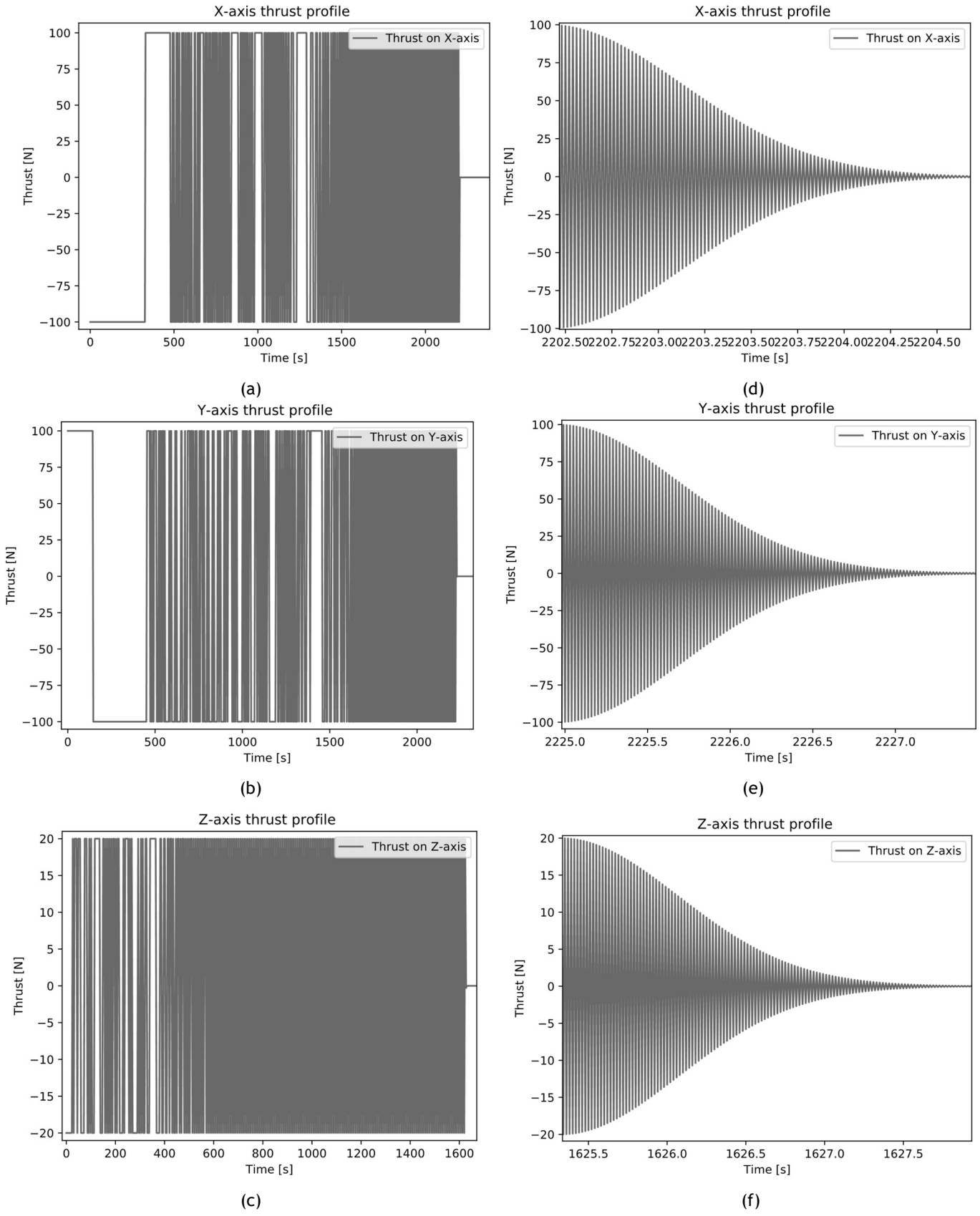

Figure 4.8: Thrust profile for each axis (a, b, c) and a closer look at the bang-bang profile (d, e, f) for the initial state $x_0 = [30000 \quad -40000 \quad 200 \quad -30 \quad 40 \quad -0.02]^T$.

4.5.3 Third example

For the last example, only the position and velocity on the z-axis are incremented by two orders of magnitude. The purpose of this example is to show that the most sensible and unstable to change axis can also be controlled while the solution $x = 0$ is found. For this reason, the initial state takes the following values

$$x_0 = \begin{bmatrix} 30000 \\ -40000 \\ 20000 \\ -30 \\ 40 \\ -20 \end{bmatrix} \quad (4.57)$$

and matrices R_1 and R_2 can be generated using the modified Bryson's method

$$R_1 = \begin{bmatrix} \frac{10^2}{30000^2} & 0 & 0 & 0 & 0 & 0 \\ 0 & \frac{10^2}{(-40000)^2} & 0 & 0 & 0 & 0 \\ 0 & 0 & \frac{10^2}{20000^2} & 0 & 0 & 9 \\ 0 & 0 & 0 & \frac{10^4}{(-30)^2} & 0 & 0 \\ 0 & 0 & 0 & 0 & \frac{1.2 \cdot 10^6}{40^2} & 0 \\ 0 & 0 & 0 & 0 & 0 & \frac{1.5 \cdot 10^4}{(-20)^2} \end{bmatrix} \quad (4.58)$$

$$R_2 = \begin{bmatrix} \frac{0.1}{100^2} & 0 & 0 \\ 0 & \frac{0.2}{100^2} & 0 \\ 0 & 0 & \frac{0.1}{20^2} \end{bmatrix} \quad (4.59)$$

Matrix $\hat{R}_2$ is created, once more, using trial and error

$$\hat{R}_2 = \begin{bmatrix} 10^{-2} & 0 & 0 & 0 & 0 & 0 \\ 0 & 10^{-2} & 0 & 0 & 0 & 0 \\ 0 & 0 & 10^{-2} & 0 & 0 & 9 \\ 0 & 0 & 0 & 1.35 \cdot 10^3 & 0 & 0 \\ 0 & 0 & 0 & 0 & 10^4 & 0 \\ 0 & 0 & 0 & 0 & 0 & 10^4 \end{bmatrix} \quad (4.60)$$

Through Euler's method, matrices P and M_2 can be calculated, using a step of $h = 0.01$

$$P = \begin{bmatrix} 9.183 \cdot 10^{-1} & 4.000 \cdot 10^{-5} & 0 & 1.700 \cdot 10^{-1} & 3.000 \cdot 10^{-5} & 0 \\ 4.000 \cdot 10^{-5} & 1.695 & 0 & 0 & 5.536 \cdot 10^{-2} & 0 \\ 0 & 0 & 4.830 \cdot 10^{-1} & 0 & 0 & 2.483 \cdot 10^{-1} \\ 1.700 \cdot 10^{-1} & 0 & 0 & 2.162 & -1.400 \cdot 10^{-3} & 0 \\ 3.000 \cdot 10^{-5} & 5.536 \cdot 10^{-2} & 0 & -1.400 \cdot 10^{-3} & 2.450 \cdot 10^{1} & 0 \\ 0 & 0 & 2.483 \cdot 10^{-1} & 0 & 0 & 1.951 \cdot 10^{1} \end{bmatrix} \quad (4.61)$$

$$M_2 = \begin{bmatrix} 5.253 \cdot 10^{1} & 1.550 \cdot 10^{-3} & 0 & 9.623 \cdot 10^{-1} & -2.100 \cdot 10^{-4} & 0 \\ 1.550 \cdot 10^{-3} & 3.112 \cdot 10^{1} & 0 & -1.300 \cdot 10^{-4} & 6.470 \cdot 10^{-1} & 0 \\ 0 & 0 & 8.062 \cdot 10^{1} & 0 & 0 & 8.562 \\ 9.623 \cdot 10^{-1} & -1.300 \cdot 10^{-4} & 0 & 1.114 \cdot 10^{2} & 1.544 \cdot 10^{-2} & 0 \\ -2.100 \cdot 10^{-4} & 6.470 \cdot 10^{-1} & 0 & 1.544 \cdot 10^{-2} & 1.633 \cdot 10^{2} & 0 \\ 0 & 0 & 8.562 & 0 & 0 & 2.569 \cdot 10^{3} \end{bmatrix} \quad (4.62)$$

and the orbital rendezvous trajectory can be generated, depicted in fig 4.9.

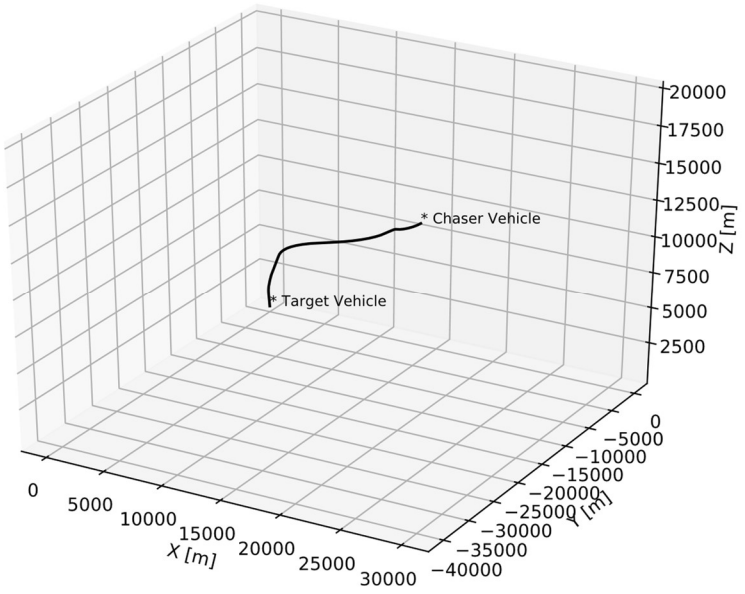

Figure 4.9: Rendezvous trajectory of the chaser spacecraft for the initial state $x_0 = [30000 \quad -40000 \quad 20000 \quad -30 \quad 40 \quad -20]^T$.

Because the relative distance on each axis has the same order of magnitude, the trajectory is not as smooth as in the previous examples. Nevertheless, the controller is still capable of finding the solution $x = 0$ to the implemented linear dynamic system. Furthermore, from fig. 4.10, this same solution is proven to be globally asymptotically stable since, when $t \to \infty$, $x(t) = 0$. Moreover, just like the previous examples, the controller applies a high rate of convergence until $t = 1000\,s$, for all axes, where it changes to a lower one. Furthermore, in this example, there is no difference in the rate of convergence, as the previous examples, between axes because all of them have the same order of magnitude.

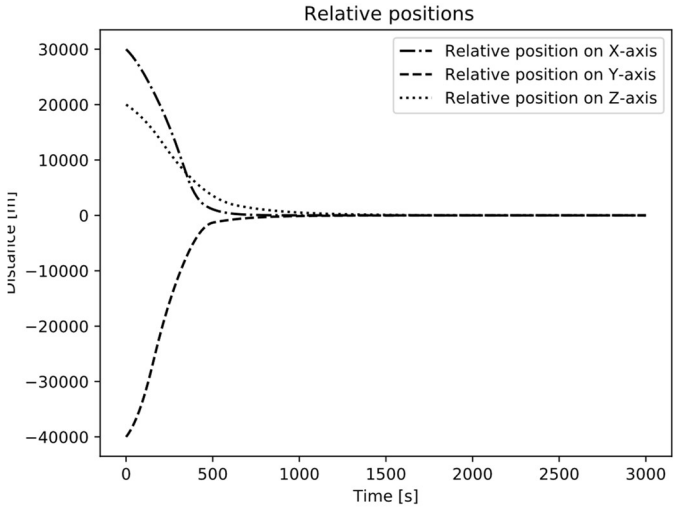

Figure 4.10: Relative position on each axis for the initial state $x_0 = [30000 \quad -40000 \quad 20000 \quad -30 \quad 40 \quad -20]^T$.

Also, the implemented nonlinear controller applies the same rate of convergence to the x-axis and y-axis. Regarding the z-axis, it takes more time to asymptotically converge to zero, until around $t = 500$ seconds, where it finally catches up. From there, all the 3 axes converge asymptotically to the solution, without overshooting the target. Regarding the thrust profile, both the x-axis and y-axis present the same shape as in the example before but the z-axis changes radically. It starts by generating -20 N for 250 seconds and it changes to 20 N after that, indicating a change in the vector's sense. After $t = 600$ seconds, the controller employs a bang-bang profile in the z-axis direction.

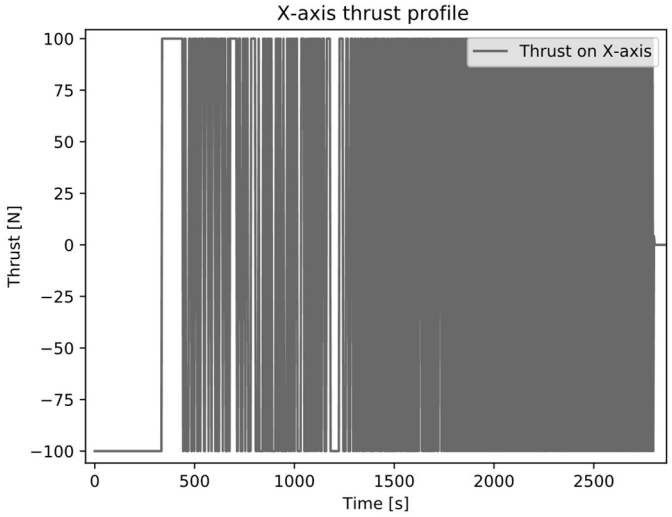

(a)

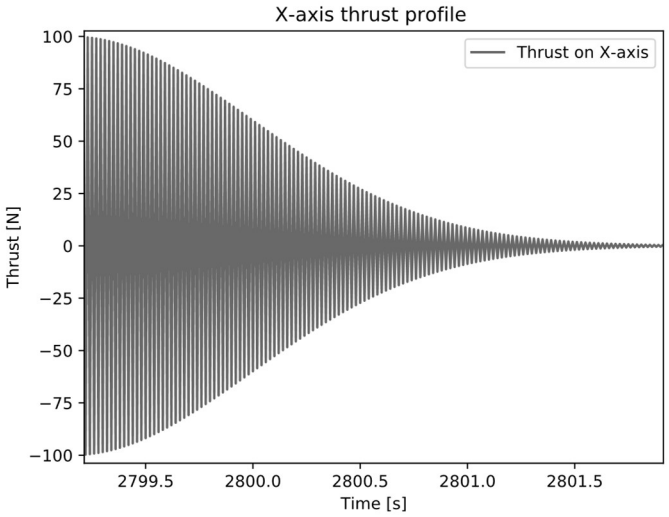

(d)

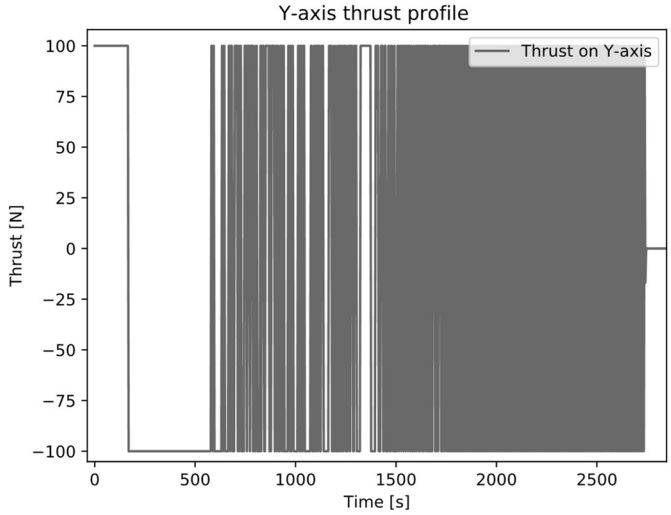

(b)

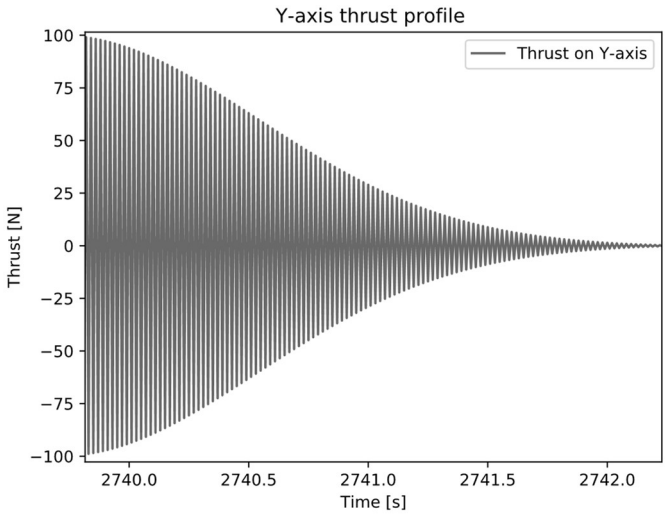

(e)

(c)

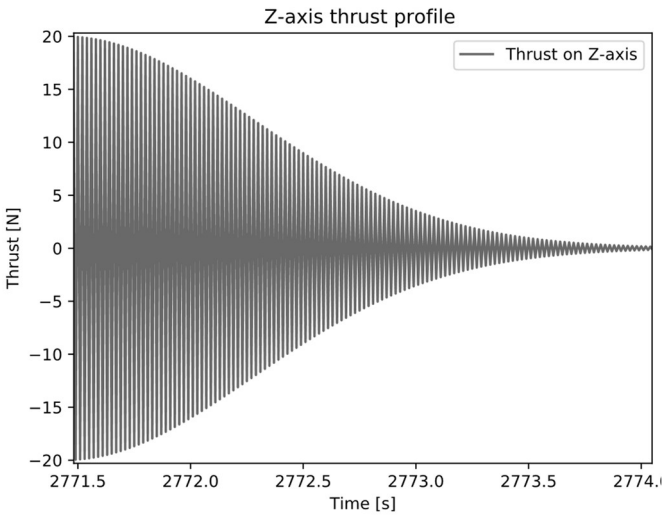

(e)

Figure 4.11: Thrust profile for each axis (a, b, c) and the bang-bang profile (d, e, f) for the initial state $x_0 = [30000 \quad -40000 \quad 20000 \quad -30 \quad 40 \quad -20]^T$.

4.5.4 Fourth example

This last example will have the same initial state matrix and matrices R_1, R_2 and $\hat{R}_2$ as the previous example. Thus, matrices P and M_2 will stay the same. Matrices A_d and B_d will change, since the norm-bounded matrix ΔA will be added to matrix A to account for perturbations in the system.

$$A_d = I + \frac{(A+\Delta A)T}{1!} + \frac{(A+\Delta A)^2T^2}{2!} + \cdots + \frac{(A+\Delta A)^nT^n}{n!} \quad (4.63)$$

$$B_d = \left(IT + \frac{(A+\Delta A)T^2}{2!} + \frac{(A+\Delta A)^2T^3}{3!} + \cdots + \frac{(A+\Delta A)^nT^{n+1}}{(n+1)!}\right)B \quad (4.64)$$

$$A_d = \begin{bmatrix} 1.000 & -1.198 \cdot 10^{-13} & 0 & 1.000 \cdot 10^{-2} & 1.149 \cdot 10^{-7} & 0 \\ 1.183 \cdot 10^{-13} & 1.000 & 0 & -1.149 \cdot 10^{-7} & 1.000 \cdot 10^{-2} & 0 \\ 0 & 0 & 1.000 & 0 & 0 & 1.000 \cdot 10^{-2} \\ 3.936 \cdot 10^{-8} & -2.396 \cdot 10^{-11} & 0 & 1.000 & 2.299 \cdot 10^{-5} & 0 \\ 2.351 \cdot 10^{-1} & 1.264 \cdot 10^{-1} & 0 & -2.299 \cdot 10^{-5} & 1.000 & 0 \\ 0 & 0 & -1.308 \cdot 10^{-8} & 0 & 0 & 1.000 \end{bmatrix} \quad (4.65)$$

$$B_d = \begin{bmatrix} 2.500 \cdot 10^{-7} & 1.915 \cdot 10^{-12} & 0 \\ -1.916 \cdot 10^{-12} & 2.500 \cdot 10^{-7} & 0 \\ 0 & 0 & 2.500 \cdot 10^{-7} \\ 5.000 \cdot 10^{-5} & 5.747 \cdot 10^{-10} & 0 \\ -5.747 \cdot 10^{-10} & 5.000 \cdot 10^{-5} & 0 \\ 0 & 0 & 5.000 \cdot 10^{-5} \end{bmatrix} \quad (4.66)$$

The resulting trajectory showed in fig. 4.12, demonstrates how the nonlinear controller deals with a system that is perturbed by an uncertainty parameter, the orbital eccentricity. By comparing fig. 4.9 with fig. 4.12, it's noticeable that there is almost no change in the trajectory.

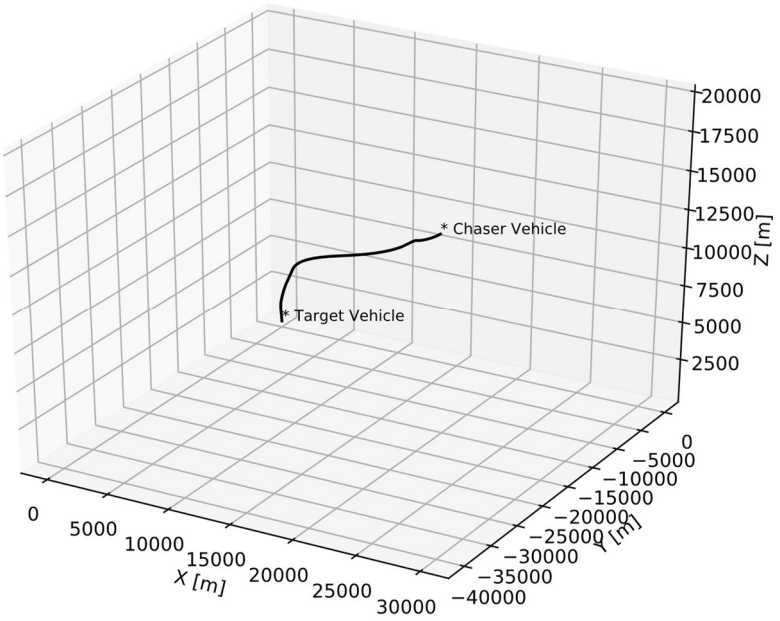

Figure 4.12: Rendezvous trajectory of the chaser spacecraft for the initial state $x_0 = [30000 \quad -40000 \quad 20000 \quad -30 \quad 40 \quad -20]^T$, with perturbation.

With fig. 4.13, the difference between the two examples is clearer. The controller takes a little longer to converge the system in the x-direction.

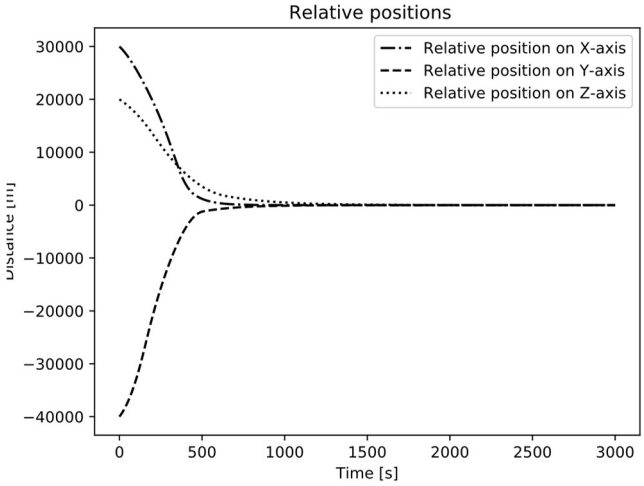

Figure 4.23: Relative position on each axis for the initial state $x_0 = [30000 \quad -40000 \quad 20000 \quad -30 \quad 40 \quad -20]^T$, with perturbation.

Looking at the thrust profile for each axis for this example, in fig. 14, it exhibits the same pattern as the previous example.

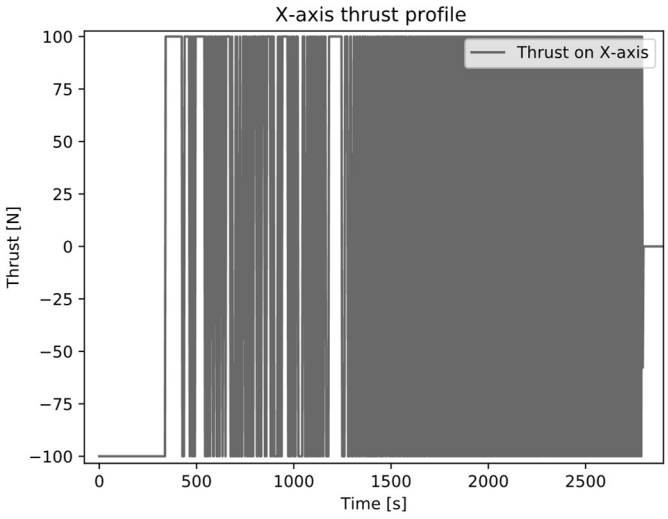

(a)

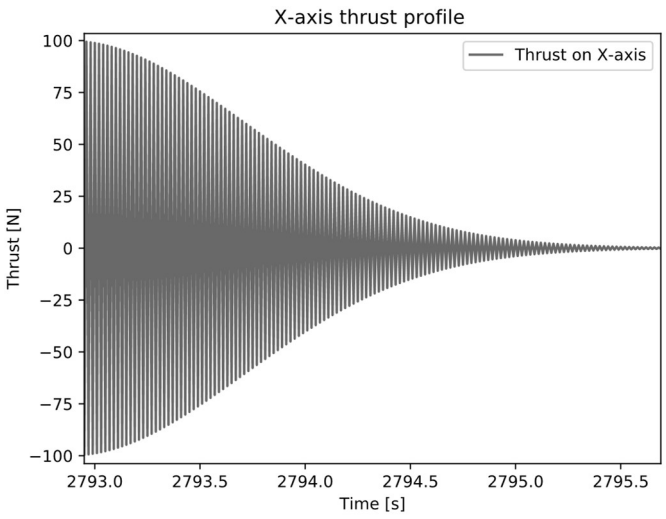

(d)

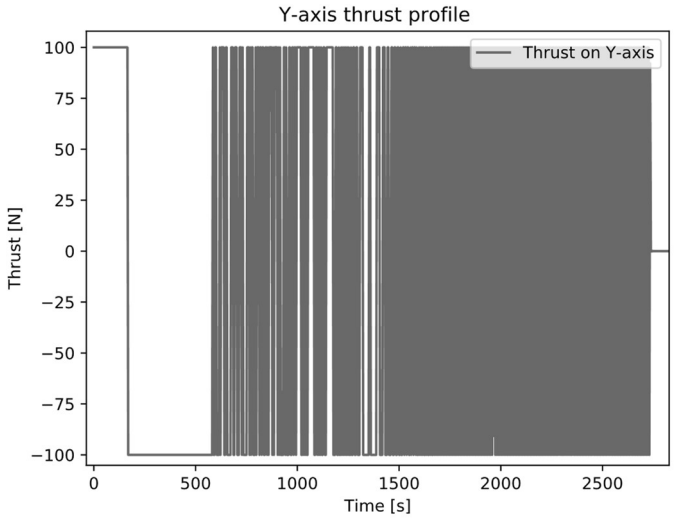

(b)

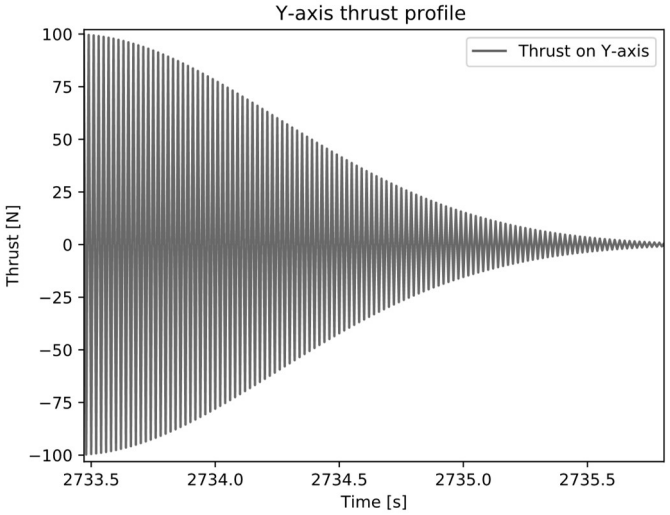

(e)

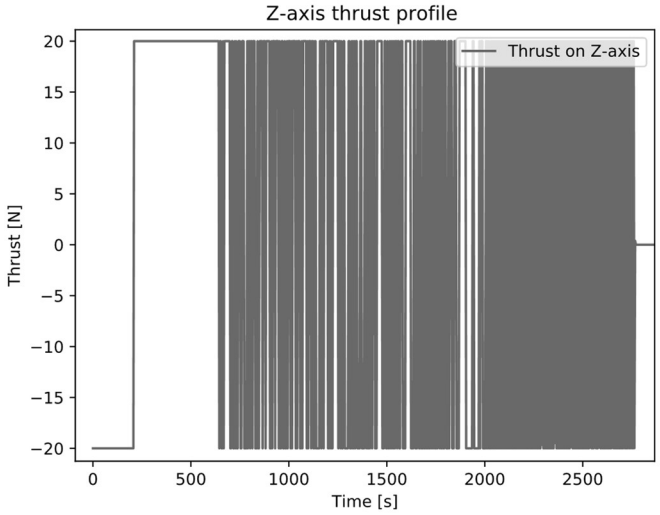

(c)

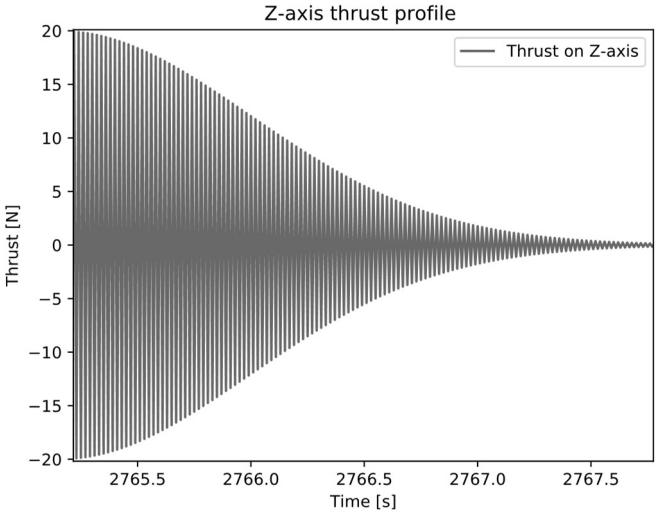

(f)

Figure 4.14: Thrust profile for each axis (a, b, c) and the bang-bang profile (d, e, f) for the initial state $x_0 = [30000 \quad -40000 \quad 20000 \quad -30 \quad 40 \quad -20]^T$, with perturbation.

Conclusion

A nonlinear control was designed to solve the orbital rendezvous problem while demonstrating robustness and performance when applied to a dynamic linear system where the chaser spacecraft performs the rendezvous maneuver in a near-circular orbit. This feedback control, based on a Lyapunov approach, was used on a linear dynamic system that uses the non-circularity of the target's orbit as an uncertainty parameter, for a wide range of relative distances and velocities, while also taking into account perturbations to the system. It was also proven that the control can, in addition, be applied to non-coplanar orbits, with great results. The four cases tested using this kind of control were able to provide the solution to the linear system, i.e., bring the chaser spacecraft to the target spacecraft, while generating a smooth trajectory with no overshooting. Even though a saturation function was used to cap the thrust produced in each direction, making it a real-world engineering problem and not only a theoretical problem, the designed algorithm could still find an asymptotically stable solution to each studied case with a reduced time frame and relatively low computer processing time. The thrust profiles for each simulation showed that the controller applies a bang-bang control, proving that this is an active rendezvous method. On all the cases presented it is also noticeable that the generated thrust is equal to zero when the controller has found a solution, demonstrating that, in fact, the controller properly works.

Regarding the control matrices, that was proven to be the most difficult task to deal with, since the methodology used to find them was through trial and error, a method based on the user's experience that is very time-consuming. Nonetheless, this method provided great results on finding those matrices given that the relative position on each direction for all examples converged smoothly with no overshooting. Only for the last two examples, the trajectory presented a little oscillation, indicating there exist control matrices better suited for them.

Overall, the controller produced satisfactory results with and without perturbations in the system, for a wide range of relative distances and velocities. Its robust stability and effectiveness were indeed demonstrated.

In the future, it is highly recommended the use of a nonlinear dynamic system to describe the problem as accurately as possible. Furthermore, a better-suited methodology to find appropriate control matrices is recommend, reducing workload and improving the overall controller performance and robustness. Additionally, it is suggested the implementation of this controller to a system under other disturbance characteristics, for instance, solar pressure and J_2 perturbations.

Bibliography

[1] D. F. Lawden, “Optimal trajectories for space navigation,” in *Optimal trajectories for space navigation*, London, 1963, pp. 96–106.

[2] P. M. Lion and M. Handelsman, “Primer vector on fixed-time impulsive trajectories,” *AIAA J.*, vol. 6, pp. 127–132, 1968.

[3] J. Wang, H. Baoyin, J. Li, and F. Sun, “Optimal four-impulse rendezvous between coplanar elliptical orbits,” in *Science China Physics, Mechanics and Astronomy*, vol. 54, no. 4, 2011, pp. 792–802.

[4] A. Miele, M. W. Weeks, and M. Ciarcià, “Optimal trajectories for spacecraft rendezvous,” *J. Optim. Theory Appl.*, vol. 132, no. 3, 2007, pp. 353–376.

[5] N. Wan, M. Liu, and H. R. Karimi, “Observer-based robust control for spacecraft rendezvous with thrust saturation,” *Abstr. Appl. Anal.*, vol. 2014, 2014.

[6] H. Gao, X. Yang, and P. Shi, “Multi-objective robust H∞ control of spacecraft rendezvous,” *IEEE Trans. Control Syst. Technol.*, vol. 17, no. 4, 2009, pp. 794–802.

[7] W. M. Haddad, V. S. Chellaboina, and J. L. Fausz, “Robust nonlinear feedback control with nonquadratic performance criteria,” *Proc. IEEE Conf. Decis. Control*, vol. 2, 1995, pp. 1982–1987.

[8] J. U. Park, K. H. Choi, and S. Lee, “Orbital rendezvous using two-step sliding mode control,” *Aerosp. Sci. Technol.*, vol. 3, no. 4, 1999, pp. 239–245.

[9] D. Lee and H. Pernicka, “Optimal control for proximity operations and docking,” *Adv. Astronaut. Sci.*, vol. 135, no. 3, 2010, pp. 225–244.

[10] R. S. Clohessy, W. H.; Wiltshire, “Terminal Guidance System for Satellite Rendezvous,” *J. Aerosp. Sci.*, vol. 27, no. 9, 1960, pp. 653-658.

[11] N. Wan, M. Liu, and H. R. Karimi, “Robust tracking control for rendezvous in near-circular orbits,” *Math. Probl. Eng.*, vol. 2013, 2013, pp-1-11.

[12] Y. Luo, J. Zhang, and G. Tang, “Survey of orbital dynamics and control of space rendezvous,” *Chinese J. Aeronaut.*, vol. 27, no. 1, 2014, pp. 1–11.

[13] A. Stoornvogel, “The H infinity control problem: a state space approach,” *Int. J. Data Min. Bioinform.*, vol. 1, 2006, pp. 77–87.

[14] G. F. Franklin, J. D. Powell, and A. Emami-Naeini, *Feedback Control of Dynamic Systems Sixth Edition*. 2010.

[15] S. Hernandez and M. R. Akella, “Lyapunov-based guidance for orbit transfers and rendezvous in levi-civita coordinates,” *J. Guid. Control. Dyn.*, vol. 37, no. 4, 2014, pp. 1170–1181.

[16] J. A. Kechichian, “Techniques of accurate analytic terminal rendezvous in near-circular orbit,” *Astrodyn. Conf. 1992*, vol. 26, no. 6, 1992, pp. 392–405.

[17] C. D. Karlgaard and F. H. Lutze, “Second-order relative motion equations,” *J. Guid. Control. Dyn.*, vol. 26, no. 1, 2003, pp. 41–49.

[18] R. Bevilacqua, M. Romano, and O. Yakimenko, “Online generation of quasi-optimal spacecraft rendezvous trajectories,” *Acta Astronaut.*, vol. 64, no. 2–3, 2009, pp. 345–358.

[19] C. M. Jewison, “Guidance and Control for Multi-stage Rendezvous and Docking Operations in the Presence of Uncertainty,” 2017.

[20] Z. Ma, O. Ma, and B. N. Shashikanth, “Optimal control for spacecraft to rendezvous with a tumbling satellite in a close range,” *IEEE Int. Conf. Intell. Robot. Syst.*, 2006, pp. 4109–4114.

[21] G. H. Moon, B. Y. Lee, M. J. Tahk, and D. H. Shim, “Optimal rendezvous guidance using linear quadratic control,” *MATEC Web Conf.*, vol. 54, 2016, pp. 1–7.

[22] M. L. Anthony and F. T. Sasaki, “Rendezvous Problem for Nearly Circular Orbits,” *AIAA J.*, vol. 3, no. 9, 1965, pp. 1666–1673.

[23] P. Lu and X. Liu, “Autonomous trajectory planning for rendezvous and proximity operations by conic optimization,” *J. Guid. Control. Dyn.*, vol. 36, no. 2, 2013, pp. 375–389.

[24] Butcher, J. (2008). Numerical methods for ordinary differential equations. Chichester: John Wiley & Sons.

[25] Fehse, W. (2003). Automated Rendezvous and Docking of Spacecraft (Cambridge Aerospace Series). Cambridge: Cambridge University Press. doi:10.1017/CBO9780511543388

[26] M. R. Caputo, “Chapter 19 - Dynamic Programming and the Hamilton-Jacobi Bellman-Equation,” *Found. Dyn. Econ. Anal. Optim. Control Theory Appl.*, 2005.

[27] V. Czitrom and J. L. Casti, “Linear Dynamical Systems,” *Technometrics*, vol. 31, no. 1, 1989, p. 125.

[28] S. Hernandez and M. R. Akella, “Lyapunov-based guidance for orbit transfers and rendezvous in levi-civita coordinates,” *J. Guid. Control. Dyn.*, vol. 37, no. 4, 2014, pp. 1170–1181.

[29] D. Pérez and R. Bevilacqua, “Lyapunov-based spacecraft rendezvous maneuvers using differential drag,” AIAA Guid. Navig. Control Conf. 2011.

[30] G. Zhang, D. Wang, X. Cao, and Z. Sun, “Tangent Orbital Rendezvous Using Linear Relative Motion with J2 Perturbations,” vol. 2013, 2013, pp-1-8.

[31] Haddad, W. and Chellaboina, V. (2008). Nonlinear dynamical systems and control. Princeton, N.J.: Princeton University Press.

[32] S. Barnett, “Linear system theory and design. By C.-T. Chen,” *Automatica*, vol. 22, no. 3, 1986, pp. 385–386.

[33] Y. Luo, J. Zhang, and G. Tang, “Survey of orbital dynamics and control of space rendezvous,” *Chinese J. Aeronaut.*, vol. 27, no. 1, 2014, pp. 1–11.

[34] Wiesel, W. (2012). Spaceflight dynamics. Beavercreek, Ohio: Aphelion Press.

Annex A

Velocity graphics for each case study

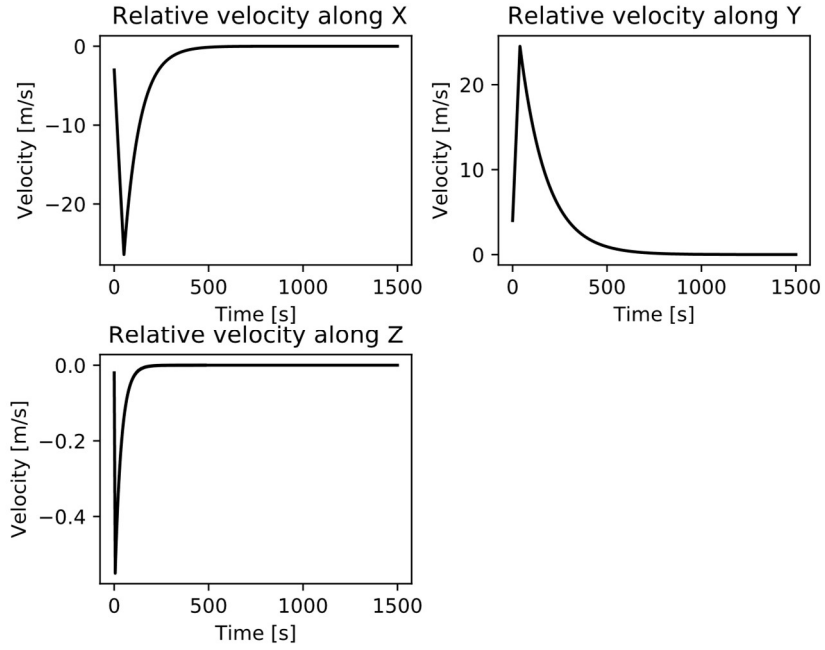

Figure A.1: Relative velocities for the initial state $x_0 = [3000 \quad -4000 \quad 20 \quad -3 \quad 4 \quad -0.02]^T$.

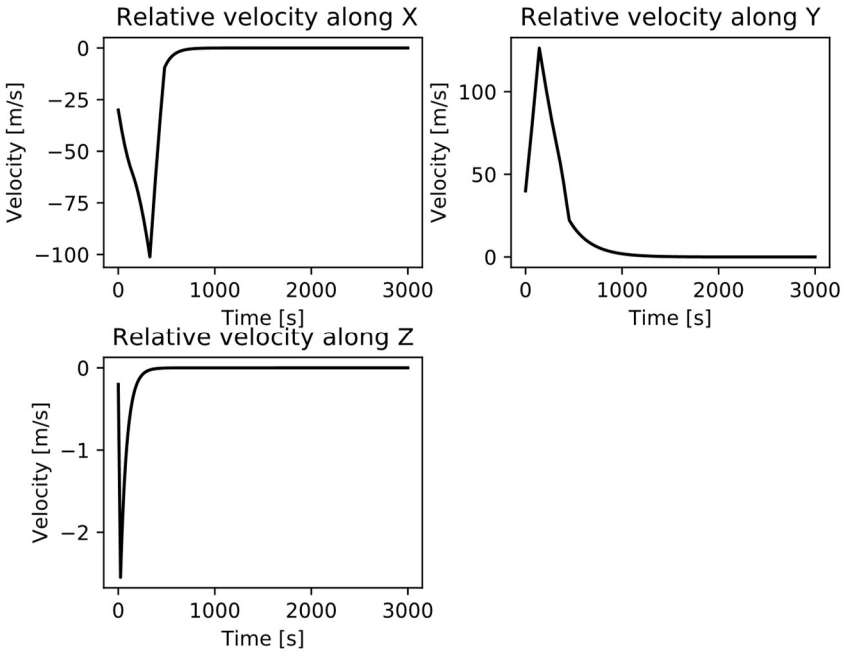

Figure A.2: Relative velocities for the initial state $x_0 = [30000 \quad -40000 \quad 200 \quad -30 \quad 40 \quad -0.2]^T$.

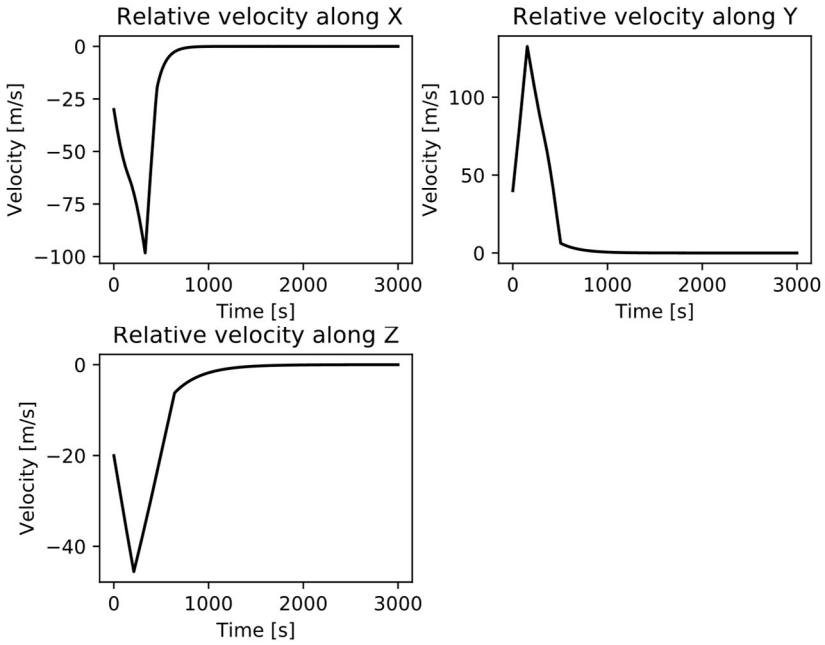

Figure A.3: Relative velocities for the initial state $x_0 = [30000 \quad -40000 \quad 20000 \quad -30 \quad 40 \quad -20]^T$.

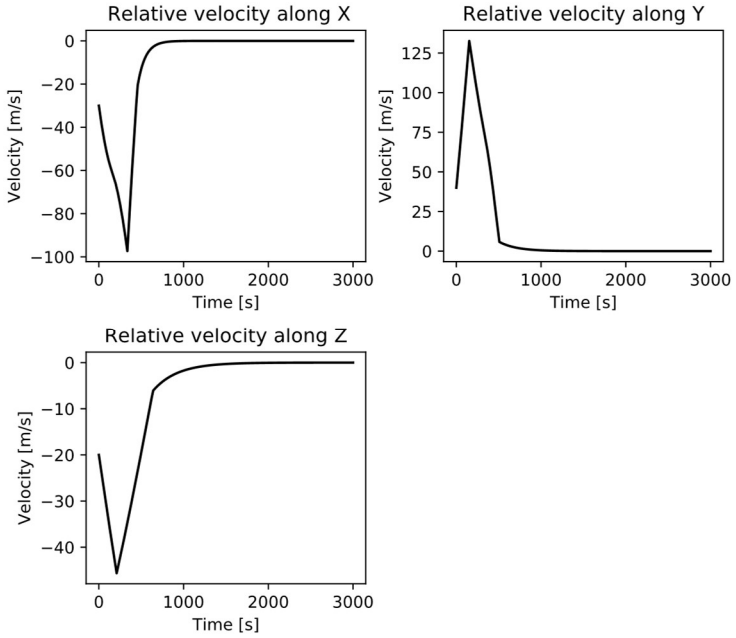

Figure A.4: Relative velocities for the initial state $x_0 = [30000 \quad -40000 \quad 20000 \quad -30 \quad 40 \quad -20]^T$, with perturbation.

Annex B

Robust nonlinear feedback control for Rendezvous in near-circular orbits

Eduardo D. Godinho.
(To be submitted to the AASS)

Robust nonlinear feedback control for Rendezvous in near-circular orbits

Eduardo D. Godinho

Abstract. This paper investigates an optimal robust guarantee nonlinear nonquadratic feedback control to address the problem of uncertain systems on orbital rendezvous missions. This control uses a based Lyapunov approach with two modified Riccati equations in order to guarantee the control robustness. A linear dynamic system is used, based on the two-body problem, with the noncircularity of the target orbit being the uncertain parameter. A saturation function is also used to make sure the control forces stay within acceptable limits. Three numerical examples are used to demonstrate the effectiveness and robustness of the nonlinear nonquadratic control with and without perturbation between non-coplanar orbits.

Keywords: Lyapunov based approach, Noncircularity, Nonlinear control, Rendezvous, Robust control.

1. Introduction

Rendezvous and docking (RND) maneuvers have always been a hard challenge to overcome throughout space missions' history. Gemini 6 and 7 were the first two spacecrafts to perform a space rendezvous. Following this remark, the Gemini 8 and the Agena Target Vehicle successfully accomplished the first manual docking. A year later, the Cosmos program achieved the first automated unmanned docking. Five decades have gone by and human intervention is still needed to successfully perform RND maneuvers. Although ground and/or astronaut onboard control is standard procedure, an effort is being made to autonomously rendezvous and dock spacecrafts. Different methodologies have been implemented to solve the rendezvous problem, usually taking the burn time and maneuver impulse to solve the trajectory design, while the propellant cost, the total time of flight or trajectory robustness is being taken into account to

optimize the process. To implement and solve the rendezvous problem, a controller must be designed. Moon et al. used a Linear Quadratic Control (LQC) to obtain the energy optimal guidance law for rendezvous missions while Miele, Weeks and Ciarcià used a sequential gradient-restoration algorithm (SGRA) to obtain time-optimal and fuel-optimal solutions for the rendezvous problem in a circular orbit. Wan, Liu, and Karimi developed a robust guaranteed cost observer-controller in near-circular orbits using the noncircularity of the target orbit as a parametric uncertainty. Furthermore, a multi-objective robust H infinity controller was also proposed to solve the rendezvous problem of two neighboring spacecrafts exposed to parameter uncertainties and external perturbations, using a Lyapunov approach. Although H infinity guarantees robustness, since it takes into consideration that the worst possible disturbance cannot destabilize the system, performance objectives may not be fulfilled such as time-optimal and/or fuel-optimal solutions. To guarantee robust stability and performance, Haddad, Chellaboina, and Fausz suggest a generalization of the classical Hamilton-Jacobi-Bellman conditions to deal with the design of robust nonlinear optimal controllers for uncertain linear systems. Such a controller is attained by modifying the nonlinear-nonquadratic performance criterion to account for system uncertainty.

The present paper studies the robustness and performance of a nonlinear nonquadratic controller applied to a rendezvous problem where the chaser spacecraft performs a rendezvous maneuver in a near-circular orbit. Based on the work of Wan et al., a first-order relative uncertain motion model in near-circular orbit is used to account for the noncircularity of the target orbit as a parametric uncertainty.

2. Problem Formulation and Dynamical Model

In this section, a nonlinear nonquadratic controller is formulated to deal with the rendezvous task.

Additionally, a relative dynamic model and a coordinate system for the rendezvous problem in near-circular orbit is established.

2.1 Problem Formulation

The present paper applies a transparent generalization of the Hamilton-Jacobi-Bellman conditions for time-invariant and infinite horizon problems to generate a nonlinear feedback controller for a nonlinear system. Also, let $\mathbb{R}$ denote real numbers and let $\mathbb{R}^{n\times m}$denote real $n \times m$ matrices. To denote $n \times n$ nonnegative and positive define matrices, the notations $\mathbb{N}^{n\times n}$ and $\mathbb{P}^{n\times n}$ are used, respectively.

Let $D \subset \mathbb{R}^n$ be an open set and let $C \subset \mathbb{R}^m$, where $0 \subset D$ and $0 \subset C$. Furthermore, let $\tilde{\mathcal{F}} \subset \{\tilde{f}: D \times C \to \mathbb{R}^n : \tilde{f}(0,0) = 0\}$represent the class of uncertain closed-loop nonlinear systems where $\tilde{f}(0,0) \in \tilde{\mathcal{F}}$ defines the nominal nonlinear system. The main task of this section is to control the
following, uncertain system

$$\dot{x} = \tilde{f}\big(x(t), u(t)\big), \;\; x(0) = x_0, \;\; t \geq 0 \tag{1}$$

where $\tilde{f}(\cdot,\cdot) \in \tilde{\mathcal{F}}$ and the control $u(\cdot)$ is limited to the class of admissible controls such that $u(t) \in U$ for all $t \geq 0$ where the control constraint set $U \subset C$ is given, with a control law $\phi(\cdot)$ that takes the form of a feedback control $u(t) = \phi\big(x(t)\big)$ and minimizes the performance functional $\tilde{J}_f(\cdot,\cdot)$from equation (3). The closed-loop system is now defined as

$$\dot{x} = \tilde{f}\left(x(t), \phi\big(x(t)\big)\right), \;\; x(0) = x_0, t \geq 0, \forall \tilde{f}(\cdot,\cdot) \in \tilde{\mathcal{F}} \tag{2}$$

It is assumed that equation (2) has a unique solution forward in time and that $\tilde{f}(\cdot,\cdot) \in \tilde{\mathcal{F}}$ is smooth and Lipschitz defined in a neighborhood of the origin $D \times C$.

2.2 Theoretical Method

The next step is to describe robust feedback controllers that guarantee robust stability over a class of nonlinear uncertain systems and minimize an auxiliary performance functional. First, let $\tilde{L}: D \times U \to \mathbb{R}$ and C define the set of asymptotically stabilizing controllers for the nominal system $\widetilde{f_0}(\cdot,\cdot)$ such that $x(\cdot)$ given by equation (1) satisfies $x(t) \to 0$ as $t \to \infty$ with $\tilde{f}(\cdot,\cdot) = \widetilde{f_0}(\cdot,\cdot)$.

Now, considering the controlled uncertain system defined above with performance functional

$$\tilde{J}_{\tilde{f}}\big(x_0, u(\cdot)\big) \triangleq \int_0^\infty \tilde{L}\left(x(t), u(t)\right) dt \tag{3}$$

and assuming $V: D \to \mathbb{R}, \tilde{\Gamma}: D \times U \to \mathbb{R}$ functions exist and a control law $\phi: D \to U$ where $V(\cdot)$ is a Lyapunov function such that

$$V(0) = 0 \tag{4}$$

$$V(x) > 0, x \in D, \;\; x \neq 0 \tag{5}$$

$$\phi(0) = 0 \tag{6}$$

$$V'^{(x)\tilde{f}(x,\phi(x))} \leq V'(x)\tilde{f}_0\big(x,\phi(x)\big) + \tilde{\Gamma}\big(x,\phi(x)\big),\ x \in D,\ \tilde{f}(\cdot,\cdot) \in \tilde{\mathcal{F}} \tag{7}$$

$$V'(x)\tilde{f}_0\big(x,\phi(x)\big) + \tilde{\Gamma}\big(x,\phi(x)\big) < 0,\ x \in D,\ x \neq 0 \tag{8}$$

$$H\big(x,\phi(x)\big) = 0,\ x \in D \tag{9}$$

$$H(x,u) \geq 0,\ x \in D,\ u \in U \tag{10}$$

where $H(\cdot,\cdot)$ is defined as

$$H(x,u) \triangleq \tilde{L}(x,u) + V'(x)\widetilde{f_0}(x,u) + \tilde{\Gamma}(x,u) \tag{11}$$

Then, there exists a neighborhood $D_0 \subset D$ of the origin such that if $x_0 \subset D_0$, the solution $x(t) = 0, t \geq 0$ of the controlled uncertain system is locally asymptotically stable or all $\tilde{f}(\cdot,\cdot) \in \tilde{\mathcal{F}}$. Furthermore, the performance functional can now be defined as

$$\tilde{J}_{\tilde{f}}\big(x_0,u(\cdot)\big) \triangleq \int_0^{\infty}\big[\tilde{L}\big(x(t),u(t)\big) + \tilde{\Gamma}\big(x(t),u(t)\big)\big]\big]\,dt \tag{12}$$

and, if $x_0 \subset D_0$, then the feedback control $u(t) = \phi\big(x(t)\big)$ minimizes the performance functional on equation (12).

To complete the statements above, if $D = \mathbb{R}^n, U = \mathbb{R}^m$ and $V(x) \to \infty$ as $\|x\| \to \infty$, then the solution $x(t) = 0, t \geq 0$ of the controlled uncertain system is globally asymptotically stable for all $\tilde{f}(\cdot,\cdot) \in \tilde{\mathcal{F}}$.

2.3 Robust feedback control of linear uncertain systems

Taking the previous statements into account, a better-suited formulation is used to deal with uncertain linear systems controlled by nonlinear controllers that minimize a polynomial cost function. Considering the following linear uncertain system

$$\dot{x}(t) = (A + \Delta A)x(t) + Bu(t),\ x(0) = 0,\ t \geq 0 \tag{13}$$

where the set of uncertain linear systems $\tilde{\mathcal{F}}$ is given by

$$\{(A + \Delta A)x + Bu : x \in \mathbb{R}^n, A \in \mathbb{R}^{n\times n}, B \in \mathbb{R}^{n\times m}, \Delta A \in \Delta\} \tag{14}$$

and $\Delta \in \mathbb{R}^{n\times n}$ is a given bounded uncertainty set of the uncertain perturbation ΔA of the nominal system A. For the uncertain linear system above, let the weighing matrices $R_1 \in \mathbb{P}^{n\times n}, R_2 \in \mathbb{P}^{m\times m}$ and $\hat{R}_k \in \mathbb{N}^{n\times n}, k = 2, \dots, r$, where r is a positive integer, be given.

Assuming there exists Ω: $\mathbb{R}^{n\times n} \to \mathbb{R}^{n\times n}$ in such a way that

$$\Delta A^T P + P\Delta A \leq \Omega(P),\ \Delta \mathrm{A} \in \Delta,\ \mathrm{P} \in \mathbb{R}^{\mathrm{n}\times\mathrm{n}} \tag{15}$$

and there exists $\mathrm{P} \in \mathbb{P}^{n\times n}, M_k \in \mathbb{R}^{\mathrm{n}\times\mathrm{n}}, k = 2, \dots, r$ in such a manner that

$$0 = A^T P + PA + R_1 + \Omega(P) - PSP \tag{16}$$

$$0 = (A - SP)^T M_k + M_k(A - SP) + \hat{R}_k + \Omega(M_k) \tag{17}$$

where $S \triangleq BR_2^{-1}B^T$. Additionally, let $\tilde{L}$ and $\tilde{\Gamma}$ be

$$\tilde{L}(x,u) = x^T\big(R_1 + \textstyle\sum_{k=3}^{r}(x^T M_k x)^{k-1}\hat{R}_k + [\sum_{k=2}^{r}(x^T M_k x)^{k-1}M_k]^T S[\sum_{k=2}^{r}(x^T M_k x)^{k-1}M_k]\big)x + u^T R_2 u \tag{18}$$

$$\tilde{\Gamma}(x,u) = x^T\big(\Omega(P) + \textstyle\sum_{k=2}^{r}(x^T M_k x)^{k-1}\Omega(M_k)\big) \tag{19}$$

Then, the linear uncertain system in equation (13) takes the performance functional

$$\tilde{J}_{\Delta A}\big(x_0, u(\cdot)\big) \triangleq \int_0^\infty \tilde{L}(x,u)\,dt \tag{20}$$

and is globally asymptotically stable for all $x_0 \in \mathbb{R}^n$ and $\Delta A \in \Delta$ with the feedback control

$$\phi(x) \triangleq -R_2^{-1}B^T[P + \textstyle\sum_{k=2}^{r}(x^T M_k x)^{k-1}M_k]x \tag{21}$$

For the present case study in this paper, a more explicit formulation is made. Firstly, let

$$\Delta \triangleq \left\{\Delta A \in \mathbb{R}^{n\times n}: \Delta\mathrm{A} = \textstyle\sum_{i=1}^{p}\sigma_i A_i\,, \sum_{i=1}^{p}\frac{\sigma_i^2}{\alpha_i^2} \leq 1\right\}, i = 1, \dots, p \tag{22}$$

where $A_i \in \mathbb{R}^{n\times n}$ are fixed matrices denoting the structure of the parametric uncertainty, α_i is an assumed positive number and σ_i is an uncertain real parameter. Secondly, let

$$\Omega(\mathrm{P}) = \textstyle\sum_{i=1}^{p}\left(\frac{\alpha_i^2}{\alpha}\right)A_i^T P A_i + \alpha P \tag{23}$$

where $\alpha = \sum_{i=1}^{p} \alpha_i$. Additionally, let

$$A_\alpha = A + \frac{\alpha}{2} I_n \tag{24}$$

where I_n denotes $n \times n$ identity matrices. For the present case study, $r = 2$ is enough to obtain the optimal robust controller and to solve the modified Riccati equations in (16)-(17).

Now, assuming there exists $P \in \mathbb{P}^{n\times n}$and $M_2 \in \mathbb{N}^{n\times n}$ and attending to the previous statements, it follows that

$$0 = {A_\alpha}^T P + P A_\alpha + R_1 + \sum_{i=1}^{p} \left(\frac{\alpha_i^2}{\alpha}\right) A_i^T P A_i - PSP \tag{25}$$

and

$$0 = (A_\alpha - SP)^T M_2 + M_2 (A_\alpha - SP) + \hat{R}_2 + \sum_{i=1}^{p} \left(\frac{\alpha_i^2}{\alpha}\right) A_i^T M_2 A_i \tag{26}$$

Furthermore, let

$$\tilde{L}(x,u) = x^T \left(R_1 + x^T M_2 x \hat{R}_2 + (x^T M_2 x)^2 M_2 S M_2\right) x + u^T R_2 u \tag{27}$$

$$\tilde{\Gamma}(x,u) = x^T \left(\sum_{i=1}^{p} \left(\frac{\alpha_i^2}{\alpha}\right) A_i^T P A_i + \alpha P + x^T M_2 x \left[\sum_{i=1}^{p} \left(\frac{\alpha_i^2}{\alpha}\right) A_i^T M_2 A_i + \alpha M_2\right]\right) x \tag{28}$$

Consequently, the linear uncertain system is globally asymptotically stable for all $x_0 \in \mathbb{R}^n$ and $\Delta A \in \Delta$ with the feedback control

$$\phi(x) \triangleq -R_2^{-1} B^T [P + (x^T M_2 x) M_2] x \tag{29}$$

2.3 Dynamical Model

The rendezvous problem implies a pre-determined meeting between two spacecrafts, the chaser and the target spacecrafts, where the two entities' relative position and velocity approximate to zero. The designations "chaser" and "target" are assigned based on the use of thrusters to perform the orbital maneuver, where the chaser is classified as "active" and the target is classified as "passive" regarding the use of its propulsion system to complete the task at hand.

To formulate the rendezvous problem a coordinate system must be chosen first. A local vertical local horizontal (LVLH) frame centered on the target spacecraft was used, where the x-

axis is directed radially outward along the position vector r, centered on Earth, the y-axis is along the velocity direction and the z-axis is normal to the reference orbit plane. Figure 1 illustrates the coordinate system described above. Following the coordinate system's description, the relative uncertain dynamic model can be expressed as

$$\dot{x}(t) = (A + \Delta A)x(t) + Bu(t) \tag{30}$$

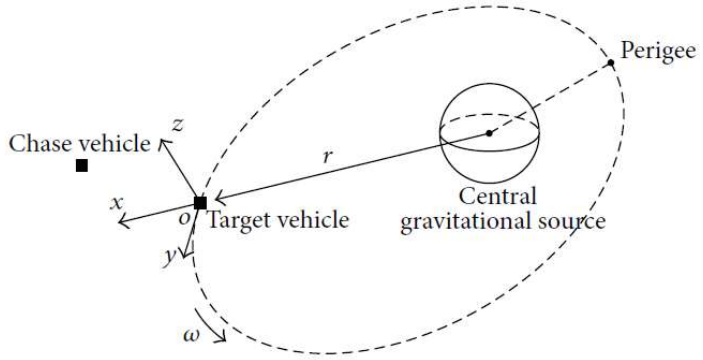

Fig.1 Local vertical local horizontal frame.

where $x(t) = [x, y, z, \dot{x}, \dot{y}, \dot{z}]^T$ is the state vector that contains the position and velocity states of the chaser spacecraft and $u(t) = \left[f_x(t), f_y(t), f_z(t),\right]^T$ is the input control vector where $f_i(t)$ for $i = x, y, z$ are the chaser's control forces along each axis. Matrices $A, \Delta A$, and B can be written as

$$A = \begin{bmatrix} 0 & 0 & 0 & 1 & 0 & 0 \\ 0 & 0 & 0 & 0 & 1 & 0 \\ 0 & 0 & 0 & 0 & 0 & 1 \\ 3n^2 & 0 & 0 & 0 & 2n & 0 \\ 0 & 0 & 0 & -2n & 0 & 0 \\ 0 & 0 & -n^2 & 0 & 0 & 0 \end{bmatrix} \quad B = \frac{1}{m}\begin{bmatrix} 0 & 0 & 0 \\ 0 & 0 & 0 \\ 0 & 0 & 0 \\ 1 & 0 & 0 \\ 0 & 1 & 0 \\ 0 & 0 & 1 \end{bmatrix}$$

$$\Delta A = \begin{bmatrix} 0 & 0 & 0 & 0 & 0 & 0 \\ 0 & 0 & 0 & 0 & 0 & 0 \\ 0 & 0 & 0 & 0 & 0 & 0 \\ 10en^2 \cos M & -2en^2 \sin M & 0 & 0 & 4en \cos M & 0 \\ 2en^2 \sin M & en^2 \cos M & 0 & -4en\, cos\, M & 0 & 0 \\ 0 & 0 & -3en^2 \cos M & 0 & 0 & 0 \end{bmatrix} \tag{31}$$

where n is the mean motion of the target spacecraft, m is the chaser's mass, e is the eccentricity of the target orbit. $M = n \cdot t_p$ is the target's mean anomaly where t_p is the time of periapsis passage. The norm-bounded matrix ΔA represents the uncertain perturbations on the target's orbit which, in the present study, is the eccentricity parameter. The present model was adopted for the

case in study since it is more accurate when compared to the nonlinear model for elliptical orbits and it is more designer-friendly.

3. Simulation Results and Discussion

In this section, two examples will be presented to demonstrate and validate the effectiveness and robustness of the nonlinear nonquadratic controller when applied to a linear uncertain system. For this simulation, the Euler method is used to calculate matrices P and M_2. The first example will simulate the controller's performance for a close relative distance (in the order of the one thousand meters) to the target spacecraft while the second example will simulate the same controller but for a greater relative distance (in the order of the ten thousand meters). The last example will use the same initial state as the second but it will use the norm-bounded matrix ΔA as perturbations to the system. For all examples, the target orbit will be the same and the chaser spacecraft will have the same mass. Also, the maximum control thrusts along the x-, y- and z-axis will be the exact same, employed by a saturation function. Table I sums up the target orbit parameters, the chaser's mass and the control thrusts used. Furthermore, the modified Bryson Method is used to, in both cases, find the most suitable R_1 and R_2. The $\hat{R}_2$ matrix is put together using trial and error to get the best results. For the parameters α_i all examples will use $\alpha_1 = 2.4 \cdot 10^{-4}$, $\alpha_2 = 1.4 \cdot 10^{-3}$, and $\alpha_3 = 1.3 \cdot 10^{-3}$, also using trial and error to get the best-suited values. Matrices P and M_2 are calculated using the Euler's Method on the modified Riccati equations (25) and (26), where both are transformed into differential equations as follows

$$\dot{P} = {A_\alpha}^T P + P A_\alpha + R_1 + \sum_{i=1}^{p} \left(\frac{\alpha_i^2}{\alpha}\right) A_i^T P A_i - PSP \tag{32}$$

$$\dot{M}_2 = (A_\alpha - SP)^T M_2 + M_2 (A_\alpha - SP) + \hat{R}_2 + \sum_{i=1}^{p} \left(\frac{\alpha_i^2}{\alpha}\right) A_i^T M_2 A_i \tag{33}$$

Both matrices are assumed to be an identity matrix for the first iteration and the process stops when $\dot{P}$ and $\dot{M}_2$ converge to zero, meaning that both matrices have converged to the solution.

Table 1 Target orbit parameters, chaser's mass and control thrusts.

Perigee distance [m]	6728140
Eccentricity	0.01
Mean motion [rad/s]	0.0013
Mean anomaly [rad]	6.378
Chaser's mass [kg]	200
Maximum control thrust along x-axis [N]	100
Maximum control thrust along y-axis [N]	100
Maximum control thrust along z-axis [N]	20

For the first example, the starting state is

$$x_0 = \begin{bmatrix} 3000 \\ -4000 \\ 20 \\ -3 \\ 4 \\ -0.02 \end{bmatrix} \tag{34}$$

and the controls matrices are

$$R_1 = \begin{bmatrix} \frac{10^5}{3000^2} & 0 & 0 & 0 & 0 & 0 \\ 0 & \frac{10^5}{(-4000)^2} & 0 & 0 & 0 & 0 \\ 0 & 0 & \frac{10^0}{20^2} & 0 & 0 & 9 \\ 0 & 0 & 0 & \frac{10^4}{(-3)^2} & 0 & 0 \\ 0 & 0 & 0 & 0 & \frac{10^4}{4^2} & 0 \\ 0 & 0 & 0 & 0 & 0 & \frac{10^0}{(-0.02)^2} \end{bmatrix} \tag{35}$$

$$R_2 = \begin{bmatrix} \frac{0.5}{100^2} & 0 & 0 \\ 0 & \frac{0.5}{100^2} & 0 \\ 0 & 0 & \frac{1}{20^2} \end{bmatrix} \tag{36}$$

$$\hat{R}_2 = \begin{bmatrix} 10^{-2} & 0 & 0 & 0 & 0 & 0 \\ 0 & 10^{-2} & 0 & 0 & 0 & 0 \\ 0 & 0 & 10^{-2} & 0 & 0 & 9 \\ 0 & 0 & 0 & 1.1 \cdot 10^3 & 0 & 0 \\ 0 & 0 & 0 & 0 & 10^3 & 0 \\ 0 & 0 & 0 & 0 & 0 & 10^2 \end{bmatrix} \tag{37}$$

and the calculated matrices P and M_2 are

$$P = \begin{bmatrix} 1.319 \cdot 10^1 & -7.000 \cdot 10^{-5} & 0 & 5.593 \cdot 10^{-1} & 6.000 \cdot 10^{-5} & 0 \\ -7.000 \cdot 10^{-5} & 8.502 & 0 & -6.000 \cdot 10^{-5} & 4.803 \cdot 10^{-1} & 0 \\ 0 & 0 & 8.491 & 0 & 0 & 1.694 \\ 5.593 \cdot 10^{-1} & -6.000 \cdot 10^{-5} & 0 & 4.717 \cdot 10^1 & 6.400 \cdot 10^{-4} & 0 \\ 6.000 \cdot 10^{-5} & 4.803 \cdot 10^{-1} & 0 & 6.400 \cdot 10^{-4} & 3.540 \cdot 10^1 & 0 \\ 0 & 0 & 1.694 & 0 & 0 & 5.005 \cdot 10^2 \end{bmatrix} \tag{38}$$

The nonlinear nonquadratic controller will stop its action course when the rendezvous is accomplished, that is, when the state vector equals 0. Fig. 2 shows the rendezvous trajectory described by the chaser spacecraft until it achieves the rendezvous task.

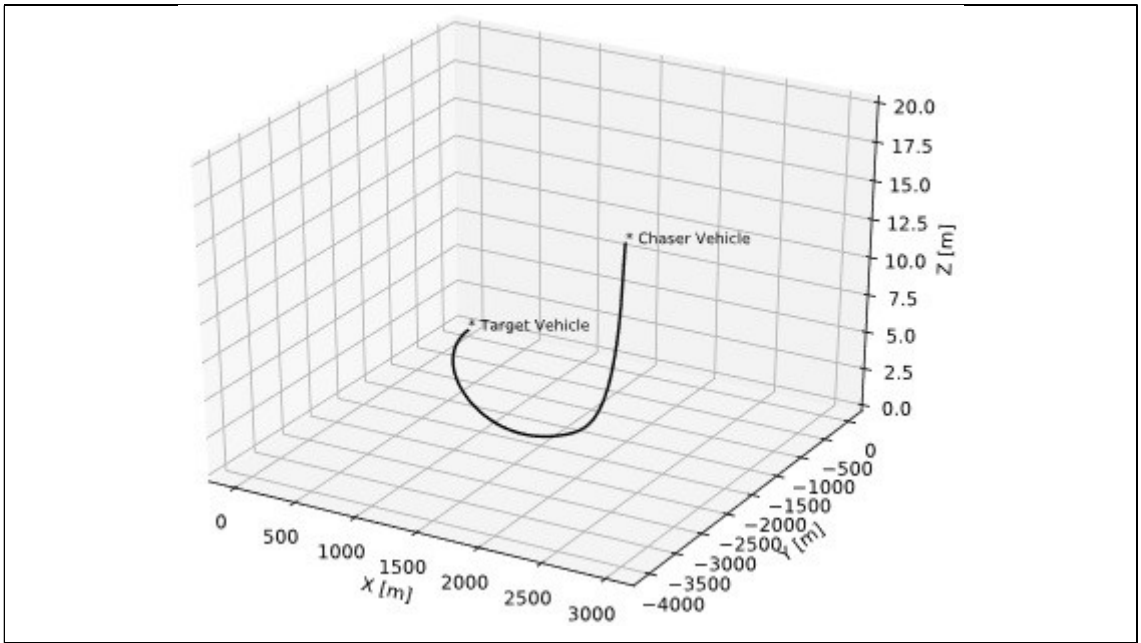

Fig.2 Rendezvous trajectory of the chaser spacecraft for the first example.

It is possible to notice that a smooth trajectory is generated by the controller applied to the linear uncertain system. Furthermore, the rendezvous task is indeed fulfilled, getting the chaser spacecraft to the target's position. A further look at Fig.3 shows the robustness and effectiveness of the controller, demonstrating the convergence to zero asymptotically.

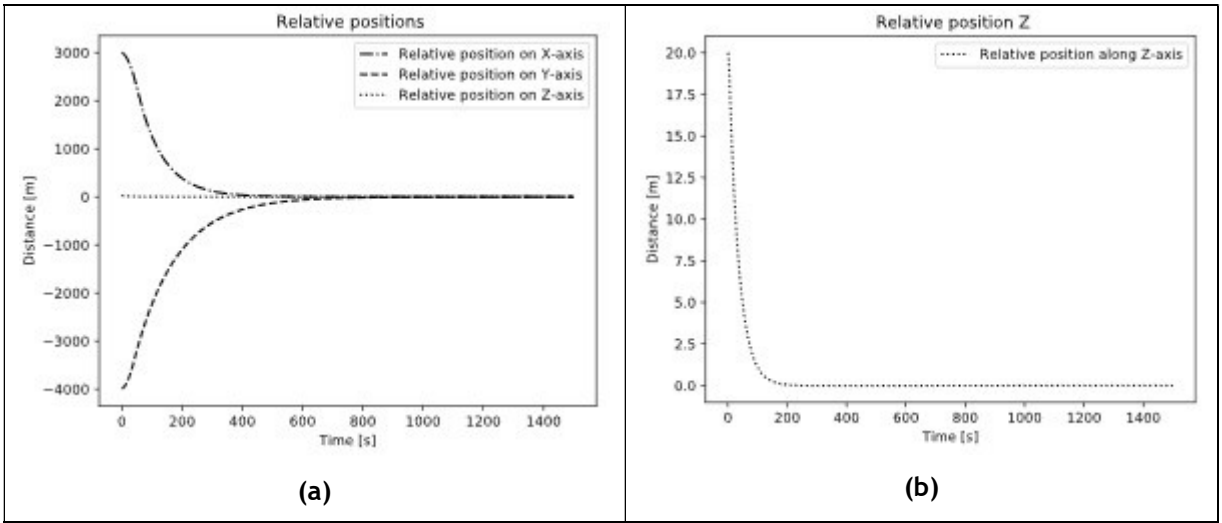

Fig. 3 Relative positions on each axis (a) and a closer look on the z-axis (b)

From Fig.4, the thrust profile can be contemplated, with its bang-bang attitude, on a closer look. The maximum control forces stipulated on the saturation function employed on the controller are working properly since none of the control forces exceed the maximum imposed value.

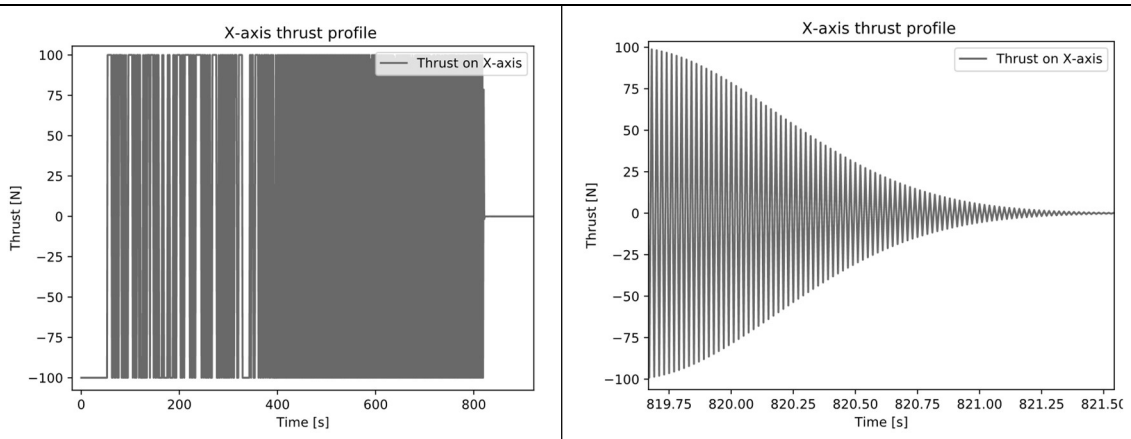

Fig. 4 Control forces of the chaser spacecraft on the x-axis (a) and a closer look at the bang-bang profile (b).

For the second example, the initial state is

$$x_0 = \begin{bmatrix} 30000 \\ -40000 \\ 20000 \\ -30 \\ 40 \\ -20 \end{bmatrix} \tag{39}$$

and the controls matrices are

$$R_1 = \begin{bmatrix} \frac{10^2}{30000^2} & 0 & 0 & 0 & 0 & 0 \\ 0 & \frac{10^2}{(-4\quad)^2} & 0 & 0 & 0 & 0 \\ 0 & 0 & \frac{10^0}{20000^2} & 0 & 0 & 9 \\ 0 & 0 & 0 & \frac{10^4}{(-30)^2} & 0 & 0 \\ 0 & 0 & 0 & 0 & \frac{10^6}{40^2} & 0 \\ 0 & 0 & 0 & 0 & 0 & \frac{10^4}{(-2\ )^2} \end{bmatrix} \tag{40}$$

$$R_2 = \begin{bmatrix} \frac{0.1}{100^2} & 0 & 0 \\ 0 & \frac{0.2}{100^2} & 0 \\ 0 & 0 & \frac{0.1}{20^2} \end{bmatrix} \tag{41}$$

$$\hat{R}_2 = \begin{bmatrix} 10^{-2} & 0 & 0 & 0 & 0 & 0 \\ 0 & 10^{-2} & 0 & 0 & 0 & 0 \\ 0 & 0 & 10^{-2} & 0 & 0 & 9 \\ 0 & 0 & 0 & 1.35 \cdot 10^{3} & 0 & 0 \\ 0 & 0 & 0 & 0 & 10^{4} & 0 \\ 0 & 0 & 0 & 0 & 0 & 10^{4} \end{bmatrix} \tag{42}$$

and the calculated matrices P and M_2 are

$$P = \begin{bmatrix} 9.183 \cdot 10^{-1} & 4.000 \cdot 10^{-5} & 0 & 1.700 \cdot 10^{-1} & 3.000 \cdot 10^{-5} & 0 \\ 4.000 \cdot 10^{-5} & 1.695 & 0 & 0 & 5.536 \cdot 10^{-2} & 0 \\ 0 & 0 & 4.830 \cdot 10^{-1} & 0 & 0 & 2.483 \cdot 10^{-1} \\ 1.700 \cdot 10^{-1} & 0 & 0 & 2.162 & -1.400 \cdot 10^{-3} & 0 \\ 3.000 \cdot 10^{-5} & 5.536 \cdot 10^{-2} & 0 & -1.400 \cdot 10^{-3} & 2.450 \cdot 10^{1} & 0 \\ 0 & 0 & 2.483 \cdot 10^{-1} & 0 & 0 & 1.951 \cdot 10^{1} \end{bmatrix} \tag{43}$$

$$M_2 = \begin{bmatrix} 5.253 \cdot 10^{1} & 1.550 \cdot 10^{-3} & 0 & 9.623 \cdot 10^{-1} & -2.100 \cdot 10^{-4} & 0 \\ 1.550 \cdot 10^{-3} & 3.112 \cdot 10^{1} & 0 & -1.300 \cdot 10^{-4} & 6.470 \cdot 10^{-1} & 0 \\ 0 & 0 & 8.062 \cdot 10^{1} & 0 & 0 & 8.562 \\ 9.623 \cdot 10^{-1} & -1.300 \cdot 10^{-4} & 0 & 1.114 \cdot 10^{2} & 1.544 \cdot 10^{-2} & 0 \\ -2.100 \cdot 10^{-4} & 6.470 \cdot 10^{-1} & 0 & 1.544 \cdot 10^{-2} & 1.633 \cdot 10^{2} & 0 \\ 0 & 0 & 8.562 & 0 & 0 & 2.569 \cdot 10^{3} \end{bmatrix} \tag{44}$$

Although the relative distance on each axis is greater than the previous example, especially on the z-axis, the resulting trajectory, in Fig. 5, shows a successful rendezvous maneuver with a smooth trajectory.

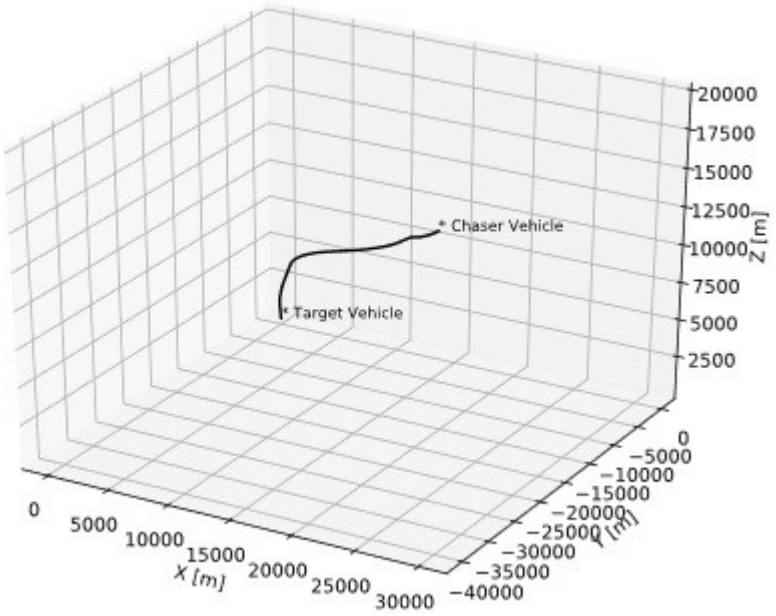

Fig. 5 Rendezvous trajectory of the chaser spacecraft for the second example.

Fig. 6 portrays the asymptotic convergence to zero on each axis, evidencing the robustness of the nonlinear feedback controller.

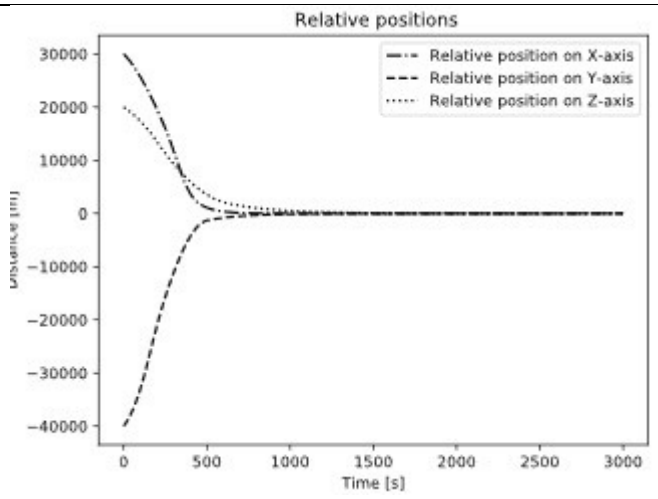

Fig.6 Relative positions on each axis for the second example.

Looking at the control forces, in Fig. 7, until $t = 400s$ the control produces $100\ N$ in the negative direction, thus the minus signal. After $t = 470s$, the controller employs a bang-bang profile to the generated thrust.

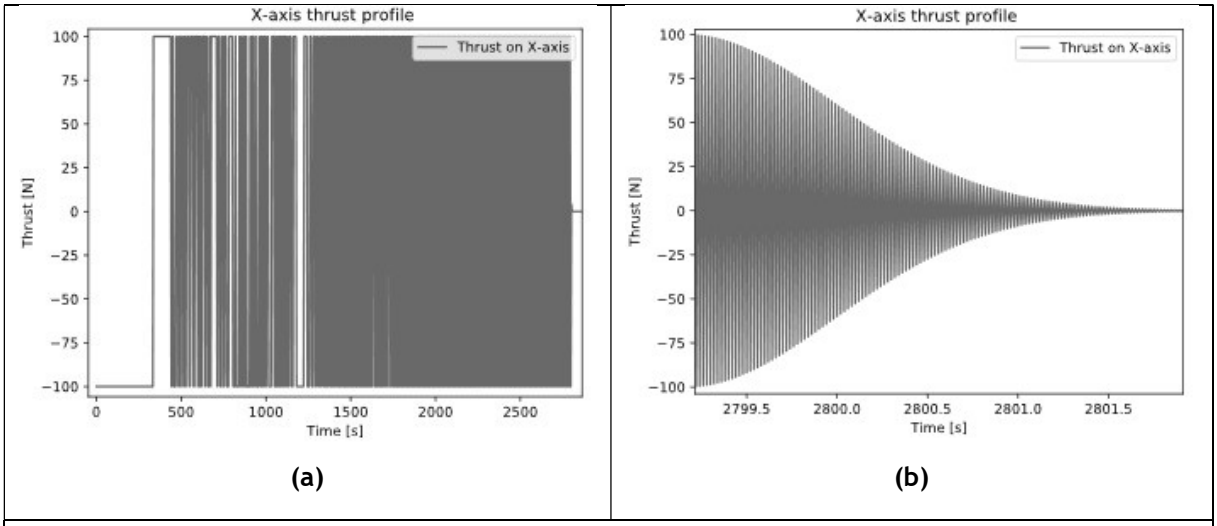

Fig. 7 Control forces of the chaser spacecraft on the x-axis (a) and a closer look at the bang-bang profile (b).

For the last example, the initial state vector will be the same as the second example, and all control matrices will remain the same. Because matrices P and M_2 only depend on those matrices they will be constant too. The norm-bounded matrix ΔA will be used as perturbation during the simulation of this example. Fig. 8 shows that even though those perturbations were added to the system, the controller can still deliver very good results

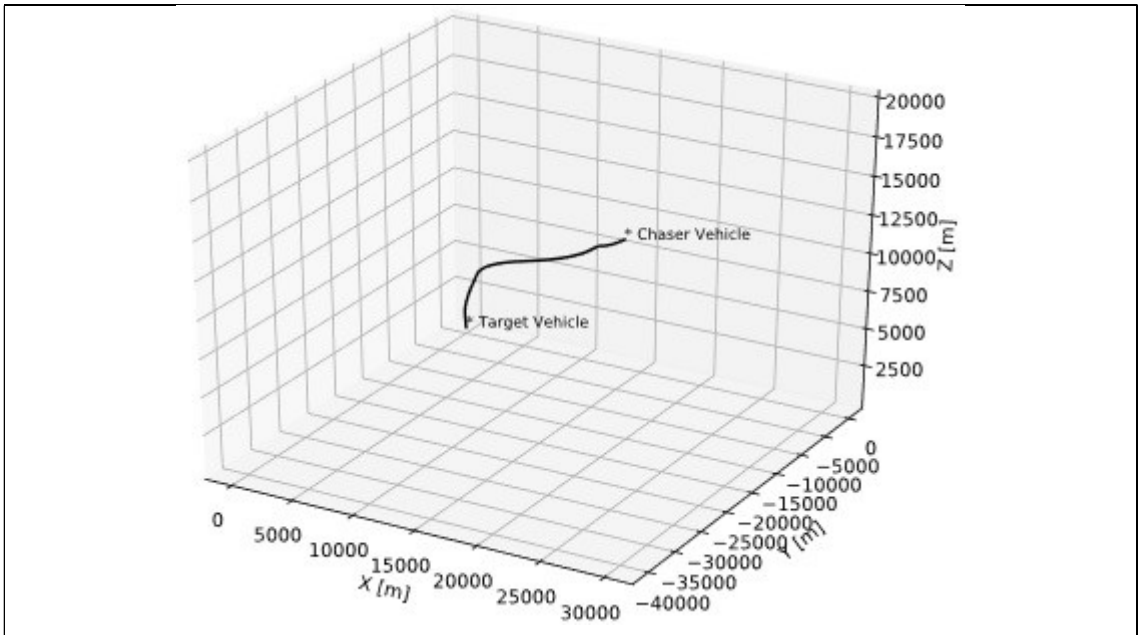

Fig. 8 Rendezvous trajectory of the chaser spacecraft for the third example.

Fig. 9 shows that the convergence process enforced by the controller, with perturbations to the system, is still smooth without overshooting the target.

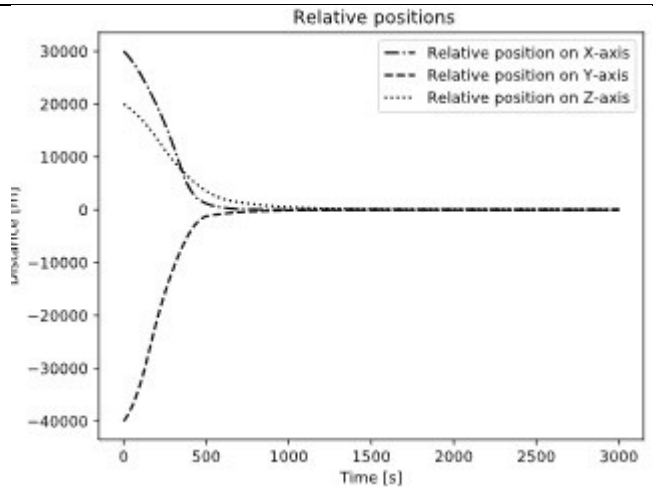

Fig.9 Relative positions on each axis for the third example.

The generated thrust for this example exhibits approximately the same profile, with no evident change in Fig. 10.

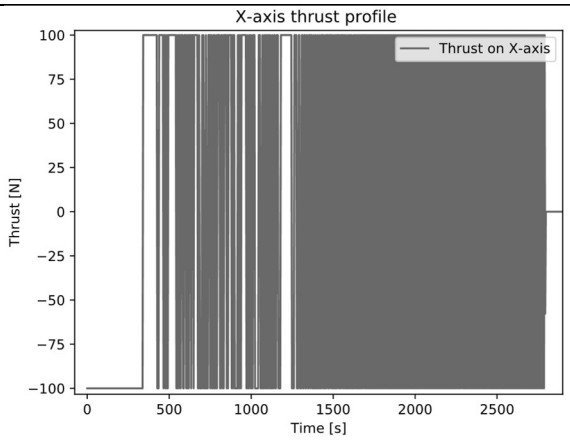

Fig. 10 Control forces of the chaser spacecraft on the x-axis for the third example.

On all the generated thrust figures, it is noticeable that the controller has stopped when the produced thrust is equal to zero, another sign that the controller can indeed fulfill the orbital rendezvous between the two vassals.

4. Conclusions

This paper has discussed a nonlinear nonquadratic controller for the spacecraft rendezvous problem. A relative dynamic model with parameter uncertainty for rendezvous in near-circular orbits has been established. An optimal controller that guarantees robust stability and performance for nonlinear and linear uncertain systems was developed by modifying the nonlinear-nonquadratic performance criterion to account for system uncertainty. Three examples were used to demonstrate the robustness and effectiveness of the controller, the first in the order of the one thousand meters and the second in the order of the ten thousand meters, showing that the nonlinear nonquadratic controller can perform well and guarantee robust stability even for large relative distances and noncoplanar orbits. The third example demonstrates that by using the uncertain parameter as a perturbation to the system, the controller can still deliver great results by generating a smooth trajectory with adequate rates of convergence in each axis.

Bibliography

Anthony ML, Sasaki FT. Rendezvous Problem for Nearly Circular Orbits. *AIAA J*. 1965;3(9):1666-1673. doi:10.2514/3.55183.

Barnett S. Linear system theory and design. By C.-T. Chen. *Automatica*. 1986;22(3):385-386. doi:10.1016/0005-1098(86)90039-7.

Bevilacqua R, Romano M, Yakimenko O. Online generation of quasi-optimal spacecraft rendezvous trajectories. *Acta Astronaut*. 2009;64(2-3):345-358. doi:10.1016/j.actaastro.2008.08.001.

Butcher, J. (2008). Numerical methods for ordinary differential equations. Chichester: John Wiley & Sons.

Di Cairano S, Pascucci CA, Bemporad A. The rendezvous dynamics under linear quadratic optimal control. *Proc IEEE Conf Decis Control*. 2012:6554-6559. doi:10.1109/CDC.2012.6426613.

Caputo MR. Chapter 19 - Dynamic Programming and the Hamilton-Jacobi Bellman-Equation. *Found Dyn Econ Anal Optim Control Theory Appl*. 2005.

Clohessy, W. H.; Wiltshire RS. Terminal Guidance System for Satellite Rendezvous. *J Aerosp Sci*. 1960. doi:10.2514/8.8704.

Fehse, W. (2003). Automated Rendezvous and Docking of Spacecraft (Cambridge Aerospace Series). Cambridge: Cambridge University Press. doi:10.1017/CBO9780511543388

Gao H, Yang X, Shi P. Multi-objective robust H∞ control of spacecraft rendezvous. *IEEE Trans Control Syst Technol*. 2009;17(4):794-802. doi:10.1109/TCST.2008.2012166.

Haddad, W. and Chellaboina, V. (2008). Nonlinear dynamical systems and control. Princeton, N.J.: Princeton University Press.

Hernandez S, Akella MR. Lyapunov-based guidance for orbit transfers and rendezvous in levi-civita coordinates. *J Guid Control Dyn*. 2014;37(4):1170-1181. doi:10.2514/1.62305.

Jewison CM. Guidance and Control for Multi-stage Rendezvous and Docking Operations in the Presence of Uncertainty. 2017.

Kechichian JA. Techniques of accurate analytic terminal rendezvous in near-circular orbit. *Astrodyn Conf 1992*. 1992;26(6):392-405.

Lawden DF. Optimal trajectories for space navigation. In: *Optimal Trajectories for Space Navigation*. London; 1963:96-106.

Lee D, Pernicka H. Optimal control for proximity operations and docking. *Adv Astronaut Sci*. 2010;135(3):225-244. doi:10.5139/IJASS.2010.11.3.206.

Lion PM, Handelsman M. Primer vector on fixed-time impulsive trajectories. *AIAA J*. 1968. doi:10.2514/3.4452.

Lu P, Liu X. Autonomous trajectory planning for rendezvous and proximity operations by conic optimization. *J Guid Control Dyn*. 2013;36(2):375-389. doi:10.2514/1.58436.

Luo Y, Zhang J, Tang G. Survey of orbital dynamics and control of space rendezvous. *Chinese J Aeronaut*. 2014;27(1):1-11. doi:10.1016/j.cja.2013.07.042.

Ma Z, Ma O, Shashikanth BN. Optimal control for spacecraft to rendezvous with a tumbling satellite in a close range. *IEEE Int Conf Intell Robot Syst*. 2006:4109-4114. doi:10.1109/IROS.2006.281877.

Miele A, Weeks MW, Ciarcià M. Optimal trajectories for spacecraft rendezvous. *J Optim Theory Appl*. 2007;132(3):353-376. doi:10.1007/s10957-007-9166-4.

Miele A, Weeks MW, Ciarcià M, Weeks MW, Ciarcià M, Weeks MW. Guidance trajectories for spacecraft rendezvous. *J Optim Theory Appl*. 2007;132(3):377-400. doi:10.1007/s10957-007-9166-4.

Moon GH, Lee BY, Tahk MJ, Shim DH. Optimal rendezvous guidance using linear quadratic control. *MATEC Web Conf*. 2016;54:1-7. doi:10.1051/matecconf/20165409002.

Park JU, Choi KH, Lee S. Orbital rendezvous using two-step sliding mode control. *Aerosp Sci Technol*. 1999;3(4):239-245. doi:10.1016/S1270-9638(99)80046-7.

Perez A, Yuan C. LQR Optimal Control and Kalman Filter Implementation for Satellite Relative Motion Manuevers. :1-4.

Pérez D, Bevilacqua R. Lyapunov-based spacecraft rendezvous maneuvers using differential drag. *AIAA Guid Navig Control Conf 2011*. 2011;(August).

Stoornvogel A. The H infinity control problem: a state space approach. *Int J Data Min Bioinform*. 2006;1:77-87. doi:10.1504/IJDMB.2006.009922.

Tiwari A, Fung J, Carson JM, Bhattacharya R, Murray RM. A framework for lyapunov certificates for multi-vehicle rendezvous problems. *Proc Am Control Conf*. 2004;6:5582-5587. doi:10.1109/ACC.2004.249029.

Wan N, Liu M, Karimi HR. Observer-based robust control for spacecraft rendezvous with thrust saturation. *Abstr Appl Anal*. 2014;2014. doi:10.1155/2014/710850.

Wan N, Liu M, Karimi HR. Robust tracking control for rendezvous in near-circular orbits. *Math Probl Eng*. 2013;2013. doi:10.1155/2013/726945.

Wang J, Baoyin H, Li J, Sun F. Optimal four-impulse rendezvous between coplanar elliptical orbits. In: *Science China Physics, Mechanics and Astronomy*. Vol 54. ; 2011:792-802. doi:10.1007/s11433-011-4289-x.

Zhang G, Wang D, Cao X, Sun Z. Tangent Orbital Rendezvous Using Linear Relative Motion with J2 Perturbations. 2013;2013.

Zhang G, Zhou D. A second-order solution to the two-point boundary value problem for rendezvous in eccentric orbits. *Celest Mech Dyn Astron*. 2010;107(3):319-336. doi:10.1007/s10569-010-9269-3.

Zhang J, Parks G. Multi-objective optimization for multiphase orbital rendezvous missions. *J Guid Control Dyn*. 2013;36(2):622-629. doi:10.2514/1.57786.